JOINT EUROPEAN TORUS JET

JET–P(93)30

O.N. Jarvis

Application of Neutron Measuring Techniques to Tokamak Plasmas

Application of Neutron Measuring Techniques to Tokamak Plasmas

O.N. Jarvis

JET-Joint Undertaking, Culham Science Centre, OX14 3DB, Abingdon, UK

Preprint of a paper to be submitted for publication in
Plasma Physics and Controlled Fusion
April 1993

ABSTRACT

The present article reviews the neutron measurement techniques that are currently being applied to the study of tokamak plasmas. The range of neutron energies of primary interest is limited to narrow bands around 2.5 and 14 MeV, and the variety of measurements that can be made for plasma diagnostic purposes is also restricted. To characterize the plasma as a neutron source, it is necessary only to measure the total neutron emission, the relative neutron emissivity as a function of position throughout the plasma, and the energy spectra of the emitted neutrons. In principle, such measurements might be expected to be relatively easy. That this is not the case is mostly a consequence of the time-scale on which the measurements have to be made and of the wide range of neutron emission intensities that have to be covered; for tokamak studies, the time scale is of order 1 to 100 ms and the neutron intensity ranges from 10^{12} to 10^{19} s^{-1}.

1. INTRODUCTION

The present article reviews the neutron *measurement* techniques that are currently being applied to the study of tokamak plasmas. It is not an introduction to the set of neutron *detection* techniques that are applicable to plasma diagnostics, which have been described elsewhere (JARVIS, 1983). The immediate objective for the neutron diagnostician is to characterize the plasma under study as a source of neutrons. Ideally, only fusion reactions between ions of deuterium and tritium will be involved, generating 2.5 and 14 MeV neutrons from the two reactions D(d,n)^{3}He and T(d,n)^{4}He. However, one frequent consequence of the application of high-power ion cyclotron resonance frequency (ICRF) heating (GRANATSTEIN and COLESTOCK, 1985) is the acceleration of light ions (p, d, ^{3}He) to such high energies (> 1 MeV) that nuclear reactions with the more abundant of the plasma impurity ions (e.g. ^{9}Be, ^{12}C) become a surprisingly strong source of neutrons over a broad energy range (SADLER et al, 1990a). This additional source must be recognized in order that erroneous conclusions regarding the effectiveness of the plasma heating can be avoided. In addition, we note the possibility of photoneutron production arising from runaway electron generation (KNOEPFEL and SPONG, 1979); this source is dominant for hydrogen-fuelled plasmas but, when deuterium fuel is used, it is only important following plasma disruptions (JARVIS et al, 1988) and will not be considered further.

The variety of neutron measurements that can be made is rather restricted. It is only possible to measure the total neutron emission strength, the relative neutron emissivity as a function of position over a poloidal section through the plasma, and the energy spectra of the neutrons emitted along selected chords through the plasma. The relevant neutron diagnostics are summarized in Table I; the information sought from the measurements is indicated and will be explained later.

Neutron diagnostics provide data that may be used directly, supplying estimates of such basic plasma quantities as fuel density and temperature. With some ingenuity, information concerning particle transport properties (particle and thermal diffusivities) can be extracted. Neutron diagnostics may also be used to test the classical nature of fast particle slowing down times and the presence or otherwise of important magneto-hydrodynamic (MHD) effects. Above all, the neutron emission is an immediate measure of the progress towards the achievement of thermonuclear reactor conditions. Somewhat paradoxically, neutron data are not used directly as input to the major plasma transport analysis codes, such as TRANSP (GOLDSTON et al, 1981), because it is straightforward to predict the neutron emission from the basic density and temperature data, supplemented by the known physics of, for example, beam-plasma interactions. Comparison of predictions (with significant associated uncertainties) with the measured neutron data (with relatively small uncertainties) then permits refinement of the input data through iterative calculations. Ohmic and neutral beam heating (CORDEY and CORE, 1974) can be modelled very well, but modelling ICRF heating (STIX, 1975) is difficult. Of course, this approach only predicts the neutron production from fusion reactions, which can be a serious limitation when ICRF heating is employed.

The main advantage of the estimates of plasma parameters derived directly from neutron measurements is that interpretation is straightforward

Table I. Neutron Diagnostic Systems

System	Comments
Time resolved neutron yield monitor.	Measures the instantaneous neutron emission strength. Distinction between D-D and D-T neutrons is necessary for triton burnup studies. Rapid signal fluctuations can be related to MHD effects. Redundancy is required to ensure complete reliability.
Activation system.	Determines absolute neutron yields and hence calibration of time-resolved neutron yield monitors for D-D and D-T neutrons.
2-D neutron camera (D and DT plasmas).	Measures radial neutron intensity distributions from two directions, from which total neutron yields can be obtained. Permits tomographic reconstruction of neutron emission. Facilitates study of triton burnup in D-plasmas, to investigate fast particle confinement and to determine n_d/n_e ratios.
Neutron spectrometers (radial and tangential).	Measurement of neutron energy spectra; permits separation of thermal and beam-plasma contributions. Indicates existence of neutron production from ICRF-heated particle interactions with impurities. Determines n_d/n_e ratios in D plasmas and n_{fuel}/n_e ratio in DT plasmas.

with well-known (if intricate) physics. The measurements are based on neutron detection techniques that are derived from work with fission reactors and in experimental neutron physics. The range of primary neutron energies of interest is limited to narrow bands around 2.5 and 14 MeV. As indicated above, the variety of measurements that are possible is restricted. In principle, they should be relatively easy to perform. That this is not the case, is mostly a consequence of the time-scale on which they have to be made and of the wide range of neutron intensities that have to be covered; for tokamak studies, the time-scale is typically of the order 1 to 100 ms and the intensity ranges from 10^{10} to 10^{19} s^{-1}. In addition, the practical difficulties associated with working in the environment of a tokamak destined for d-t operation should not be under-estimated.

The remainder of this article is devoted to reviewing the neutron measuring techniques in use at existing large tokamaks, as summarized in Table II. Section 2 provides some necessary theoretical background information. Section 3 is devoted to the measurement of time-resolved neutron yields that is practised at almost all tokamak installations, large or small. Section 4 is concerned with precise measurements of time-integrated yields, which constitute a powerful method for calibrating the time-resolved instrumentation. Section 5 deals with the measurement of neutron emission profiles; until now, such measurements have been undertaken only at TFTR and JET. Section 6 deals with neutron spectrometry, which has been investigated at several tokamaks but has

Table II. The range of neutron diagnostics installed on high current (> 1 MA) tokamaks constructed for deuterium operation.

Tokamak	Time-Resolved Neutron Counters (no energy selection) (No. of positions)	Time-Resolved Neutron Counters (14 MeV neutrons only) (No. of positions).	Activation System (No. of positions)	Profile Monitor (No. of channels, Vertical or Horizontal)	Spectrometer (d-d or d-t)
JET	3	2	8	9V, 10H	2d-d, 2d-t
DIII-D	^{3}He prop.	1	no	no	no
JT-60U	3	1	1	no	d-d
TFTR	4	1	4	10V	d-d
Asdex-U	1	(1-planned)	(3-planned)	no	d-d
Tore Supra	yes	no	no	no	no
FTU	3	no	2	(5V- being constructed)	no
T-15	4	no	2	no	d-d

See Nuclear Fusion Special Supplement 1991 for a full listing of tokamaks world-wide.

been applied systematically only at JET. The basic techniques of neutron detection are not discussed, having been covered more thanadequately in books such as that of KNOLL (1989). For reasons of accessibility for the author, most of the examples of experimental data are drawn from measurements performed at JET,

where the most extensive set of neutron diagnostics is in use. The related topics of measurement of gamma-radiation emitted from fusion and nuclear reactions occurring between ions inside the plasma, and of charged fusion product diagnostics, are not reviewed because of space limitations.

Useful references to prior work include the rather complete review of plasma diagnostics on large tokamaks by ORLINSKIJ and MAGYAR (1988) and the very extensive fusion product bibliography compiled by H-S BOSCH (1991). For general reading, the proceedings of the Diagnostics Workshops held in Varenna, Italy, (e.g. see JARVIS, 1983) and those of the American Physical Society Topical Conferences on High Temperature Diagnostics (published in the Review of Scientific Instruments) are recommended.

2. THEORETICAL BACKGROUND.

2.1 Fusion reactions.

The fusion reactions of principal interest are the following:

D + D	$\rightarrow$ t (1.011 MeV) + p (3.022 MeV)	Q = 4.033 MeV	(1)
D + D	$\rightarrow$ ^{3}He (0.820 MeV) + n (2.449 MeV)	Q = 3.269 MeV	(2)
t + D	$\rightarrow$ ^{4}He + n	Q = 17.589 MeV	(3a)
D + T	$\rightarrow$ ^{4}He (3.561 MeV) + n (14.029 MeV)	Q = 17.589 MeV	(3)
T + T	$\rightarrow$ ^{4}He + 2n	Q = 11.332 MeV	(4)

In the above equations, the hydrogenic species are represented by upper case letters for reacting thermal ions and by lower case letters for energetic fusion products. The particle energies for zero energy reactants are given within parentheses, if appropriate; also, the reaction Q-values are provided. The two branches of the D-D reaction occur with nearly equal probability; the ratio of the cross-sections for the proton and neutron branches are given by BOSCH and HALE (1992) in the following polynomial form:

$$BR = \sigma_{ddp}/\sigma_{ddn} = 1.04305 - 2.6573\times10^{-3}E + 1.2923\times10^{-5}E^2 - 2.4454\times10^{-8}E^3$$

where E is the energy available between the reacting ions in the centre-of-mass frame, in keV. The formula is valid only for energies below 100 keV.
Equation 3a, above, relates to the fusion reactions undergone by the *circa* 1.0 MeV fusion product tritons emitted from the first branch of the D-D reaction; the

reaction cross-section for triton burnup increases as the triton slows down in the plasma, reaching a maximum at a laboratory energy of 165 keV, after which it falls rapidly. Triton burnup is a particularly valuable area for study, since the emission of 2.5 MeV neutrons can be taken as signaling the birth of a triton population, while the observation of the 14 MeV neutrons provides information on the confinement, slowing down time and radial movement of these tritons. The 1 MeV tritons have Larmor radii close to those of the 3.5 MeV alpha-particles emitted from D-T reactions, and therefore exhibit similar slowing down, diffusion and confinement properties. Study of the fusion product tritons therefore permits the probable single-particle behaviour of alpha-particles to be determined prior to the introduction of tritium into tokamaks.

2.2 Fusion reaction cross-sections

The strong dependence of the fusion reaction cross-sections with particle energy is illustrated in fig. 1. Reliable experimental cross-section data (BROWN et al, 1987 and 1990) are not available for energies below about 15 keV. Since calculations of fusion reaction rates for use in fusion research involves a knowledge of the reaction cross-sections for far lower energies, it is necessary to extrapolate downwards using the theoretical formula for two charged particles of mass m_1 (projectile) and m_2 (target):

$$\sigma(E) = \frac{S(E)}{E}\exp(-R/\sqrt{E}), \text{ with } R = \pi\left(\frac{e^2}{\hbar c}\right)\sqrt{2\mu c^2}Z_1Z_2$$

where the centre-of-mass energy, E, is used, $=m_1m_2/(m_1+m_2)$ is the reduced mass and Z_1 and Z_2 are the atomic numbers. $S(E) = A\exp(-\beta E)$ and the remaining quantities have their usual meaning. Laboratory energies may be used if the substitution $E_{lab}=(m_1/m)E$ is made. The parameters A, β and R are given in Table III. This formula applies only for energies well below the Coulomb barrier. BOSCH and HALE (1992) have provided improved formulas for the fusion cross-sections applicable at higher energies, where more complex parametrizations of the S-functions are needed. In order to utilize all the available experimental data for a given mass system, R-matrix theory is employed (LANE and THOMAS, 1958).

Table III. Low energy cross-section parametrization

Reaction	A (barn-keV)	β (keV^{-1})	R ($keV/2$)
$D\text{-}D_p$	52.6	-5.810^{-3}	31.39
$D\text{-}D_n$	52.6	-5.810^{-3}	31.39
D-T	9821	-2.910^{-2}	34.37
T-T	175	9.610^{-3}	38.41

2.3 Fusion reactivities

The reaction rate per unit volume between two ion species with densities n_i and n_j is given by $r = \frac{n_i n_j}{(1+\delta_{ij})} < \sigma v >$, where the fusion reactivity, $< \sigma v >$, is the appropriate average of the fusion cross-section, σ, over the relative velocities, v, and δ_{ij} is the Kronecker delta function. The fusion reactivity is obtained after performing a six-fold integration over the components of the velocity vectors for the two interacting ions. This integration can be simplified by symmetry arguments for special cases. The dependence of the fusion reactivity on ion temperature is shown in fig. 2 for a plasma in thermal equilibrium.

Approximate formulae for the reactivity at low temperature can be derived analytically for the Maxwellian ion energy distribution (thermal equilibrium). Thus, for low energies where the cross-sections have the simple form

$$\sigma(E) = \left(\frac{A}{E}\right)\exp\left(-\beta E - \frac{R}{\sqrt{E}}\right),$$

the integration can be performed by saddle-point evaluation to give

$$< \sigma v >= 0.8052 \times 10^{-22} \frac{A R^{1/3} m^{-1/2} T^{-2/3}}{(1+\beta T)^{5/6}} . \exp\left[-3\left(\frac{R^2}{4}\right)^{1/3} (1+\beta T)^{1/3} T^{-1/3}\right]$$

in $m^3 s^{-1}$, where m is the reduced mass in a.m.u and the temperature T is in keV. It is customary to set terms involving β to unity. The low temperature formula for the fusion reactivity simplifies to

$$< \sigma v >= \kappa T^{-2/3} \exp\left(-\lambda T^{-1/3}\right),$$

from which follows the greater simplification $<\sigma v> \approx \kappa T^{\gamma}$. This dependence is frequently assumed for analytical calculations; however, it should not be forgotten that γ is itself temperature dependent:

$$\gamma = \frac{d\ln(<\sigma v>)}{d\ln(T)} = \frac{x}{T^{1/3}} - \frac{2}{3},$$

with constant x=6.27 for the D-D reaction and 6.66 for the D-T reaction. This relationship is useful only for scoping studies. When greater accuracy is required, the full parametrized forms for the fusion cross-sections should be used without approximation. Fig. 3 shows the actual variation of γ with temperature for both D-D and D-T reactions.

BOSCH and HALE have provided convenient parametrized forms for the thermal reactivities. More generalized ion energy distributions, representing neutral beam or ion cyclotron resonance heating, can be derived from Fokker-Planck calculations. Full numerical calculations, involving integrations over several velocity components, have then to be undertaken to derive the fusion reactivities.

2.4 Neutron energy spectra

The mean energies and energy distributions of neutrons emitted from D-D and D-T plasmas provide information on the ion energy distributions of the interacting ions. For the special case of Maxwellian distributions, they provide a measure of the ion temperature. As shown most directly by BRYSK (1973), the energy distribution of the neutrons is very nearly gaussian in form

$$f(E_n) = \frac{1}{W\sqrt{\pi}} \exp\left[-\frac{\{E_n - <E_n>\}^2}{W^2} \right]$$

with

$$W = \left[\frac{4 m_n <E_n> T}{m_n + m_\alpha} \right]^{1/2}.$$

The distribution full width at half maximum, *fwhm*, is $F = 2W\sqrt{\ln 2}$. The shift in $<E_n>$ with temperature is very small,

$$<E_n> = \frac{1}{2} m_n <V^2> + \frac{m_\alpha}{(m_n + m_\alpha)} (Q + K_r),$$

where V is the velocity of the centre-of-mass, Q is the reaction Q-value and K_r is the mean relative kinetic energy of the reacting pairs. The shape and spread of the neutron energy distribution are more easily measured quantities, and provide a viable diagnostic technique for determining the temperature of an approximately maxwellian plasma.

The ion temperature is readily derived from the *fwhm*, F, of the gaussian-shaped spectrum; the relationship at low ion temperatures is $F = 82.6\sqrt{T_i}$ for D-D neutrons and $F = 177.2\sqrt{T_i}$ for D-T neutrons, where F and T_i are in keV. The multipliers are weakly temperature-dependent (van BELLE and SADLER).

For non-maxwellian plasmas, but with isotropic ion velocity distributions, the neutron energy distribution is always very nearly gaussian, as shown by SLAUGHTER (1986). However, for a tokamak plasma, where there is a magnetic field with a well-defined structure, the velocity distributions will not, in general, be isotropic and the neutron energy spectrum recorded with a spectrometer will depend on the pitch-angle distribution of the ions, as determined by the angle to the field lines at which beam ions are injected or by the consequences of ICRF heating, and also on the viewing angle subtended by the spectrometer. Thus, the energy spectra recorded by a spectrometer viewing the plasma orthogonally to the field lines may differ from that recorded for a tangential view. The FPS-code of van BELLE and SADLER (1986) may be used to compute fusion product energy spectra for colliding ions possessing entirely general velocity distributions and for any desired viewing angle.

3. TIME-RESOLVED NEUTRON EMISSION

The basic requirement is to measure the absolute magnitude of the total neutron emission strength, without being unduly concerned with the neutron energy. This is acceptable for tokamaks operating with deuterium plasmas because the emission is dominated by the 2.5 MeV D-D neutrons. Likewise, when operation commences with comparable admixtures of deuterium and tritium, the emission will be dominated by the 14 MeV neutron emission. Since it is not possible to design a simple detector that will detect 2.5 MeV neutrons but not 14 MeV neutrons, it is convenient to design it to have an energy dependence that is effectively flat from very low energies to well above 14 MeV. Fortunately, it is relatively easy to design a detector that responds selectively to 14 MeV neutrons

in the presence of stronger yields of 2.5 MeV neutrons; such detectors have important applications, as will be discussed below.

Even when pure deuterium fuelling is employed, there will always be a small fraction of 14 MeV neutron emission from fusion product triton burnup (t - D) reactions. This fraction is typically between 0.2 and 2%. Measurement of these 14 MeV neutrons is important in that it enables the transport properties of the fast tritons to be studied. Significantly, experimentation has already begun (JET TEAM, 1992) with injection of tritium beams into a deuterium plasma, so that simultaneous measurements (JARVIS, 1992) of D-D and D-T neutrons permit the beam deposition and particle transport properties of tritium relative to deuterium to be studied.

The necessary time-resolution is determined by the duration of the plasma discharge or the need to investigate rapid phenomena; at JET, a routine sampling frequency of 5 ms is adequate for discharges that generally last for 30 s. Higher time-resolution is needed if it is proposed to study the effects of sawtooth internal disruptions (the sawtooth crashes occur on a time-scale that depends on the size of the machine and is of the order of 100 μs for JET); even higher time-resolution is needed to study rapid fluctuations in plasma parameters. For such measurements, neutron detectors employing moderators cannot be used (100 μs moderation times) and, instead, they are likely to be based on large volume scintillation counters working in current mode (HEIDBRINK, 1986); these will not be discussed further.

In this section, we will be concerned with rather simple detectors that can cover a wide dynamic range of intensity. As will be seen later, it is also possible to construct a neutron profile monitor that not only gives a good measure of the instantaneous neutron yield, but may be independently calibrated and can identify 14 MeV neutrons in the presence of a stronger flux of 2.5 MeV neutrons.

3.1 2.5 and/or 14-MeV neutrons

The near-instantaneous neutron emission strength is most conveniently recorded with BF_3 or ^3He proportional counters or with ^{235}U fission chambers, all of which exploit large thermal reaction cross-sections and are therefore embedded in polythene moderators to thermalize the incident neutrons. These neutron monitors exhibit no neutron energy discrimination properties, other than

rejection of incident thermal neutrons by capture in a surrounding thin layer of cadmium. They can, however, be engineered so as to offer an essentially flat energy response, as mentioned earlier. They are usually located close to the tokamak so as to sample neutrons from a major portion of the plasma. The sensitivity of BF_3 and ^3He counters is such that they can record typically one event for every 10^6 neutrons emitted. At TFTR (HENDEL and JASSBY, 1990), JT-60U (NISHITANI et al, 1992) and JET (JARVIS et al, 1985), ^{235}U counters containing about 1 g of fissile material offer a sensitivity of about 1 event per 10^8 neutrons; these counters are entirely adequate for machines operating with deuterium fuel. However, it is noteworthy that at TFTR one counter loaded with about 18 g of ^{235}U is available for very low yield plasmas and to provide higher efficiency for in-vessel calibration work (see below).

For machines operating with hydrogen, the neutron emission strength will be low ($<10^{10}$ s^{-1}) and the neutron emission may, at times, be dominated by electrodisintegration of the deuterium naturally present in hydrogen and by the photonuclear reactions, both of which are associated with runaway electron generation as discussed by HENDEL and JASSBY, (1990). BF_3 or ^3He proportional counters will usually be employed because of their higher detection efficiencies. They are operated in pulse-counting mode only. The efficiency can be further raised by operating several detectors in parallel within a single moderator block; alternatively, it can be lowered by inserting a partial screen of cadmium into the moderator.

With deuterium fuelling, the higher neutron yields are best measured with fission chambers. Here, pulse counting or current sampling modes may be used. Alternatively, as at TFTR and JT-60U, the Campbelling technique (ENGLAND et al, 1986) may be adopted; this method involves determining the mean-square fluctuation in amplitude (voltage) of the recorded signal so as to emphasize the contribution from fission events (about 20 MeV deposition energy equivalent) in the presence of an intense gamma-ray signal (at the keV level per event); it is commonly applied to fission reactor measurements at low power, where there may be no relationship between the background gamma-radiation flux and the fission neutron flux. The Campbelling technique requires repetitive measurements at a frequency of some tens of kHz; it is therefore unsuitable for measurements of brief ($<100\mu s$) signal excursions, such as are encountered during sudden plasma disruptions (JARVIS et al, 1988).

When deuterium-tritium fuelling is employed, even a 1g ^{235}U chamber used in current or Campbelling mode will risk saturation. An obvious solution is then to use a ^{238}U chamber instead. Since ^{238}U exhibits a threshold energy for induced fission at about 1 MeV, there is no need for any moderator. In pulse-counting mode, the sensitivity to 14 MeV (or 2.5 MeV) neutrons from a tokamak is about 1 event per 10^{12} emitted neutrons. The factor of 10^4 difference in sensitivity between ^{235}U and ^{238}U chambers containing the same quantities of ^{235}U or ^{238}U is excessive; a factor of 100 would be more convenient. Incidentally, calibration with monoenergetic neutrons from a particle accelerator will show the intrinsic sensitivities to differ by a factor of 10^3 only, the extra factor of 10 is a consequence of the transport of neutrons in the tokamak environment. Another problem with ^{238}U counters arises when the chamber is used in current mode, since the small 2.5 MeV neutron fission cross-section (0.5 barns) results in a chamber current that is likely to be less than that drawn as a result of the gamma-radiation background. (With ^{235}U chambers, which rely on the 502 barn thermal cross-section, the gamma-radiation contribution is negligible). Surrounding the ^{238}U chamber with a substantial thickness of lead to shield out the background radiation is not a complete solution because some of the incident neutrons will suffer inelastic scattering, thermalization and capture in the lead, thereby producing a new source of gamma-radiation. This may not be a worry, since this new source is linearly dependent on the neutron flux and so provides a perfectly valid measure of that flux; nevertheless, this situation is potentially confusing and is aesthetically unsatisfying. Employment of the Campbelling technique constitutes one solution. Alternatively, the ^{238}U chambers could be discarded in favour of very small ^{235}U chambers, with about 0.01 g of fissile material and a corresponding reduction in electrode area so as to minimize the sensitivity to gamma-radiation .

Fig. 4 shows the time dependence of the neutron emission for the D-D plasma discharge (No. 26087) giving the record 2.5 MeV neutron emission at JET. The results of a TRANSP simulation are shown, along with the predicted breakdown of neutron production into contributions from thermal, beam-thermal and beam-beam fusion reactions. The detector was a ^{235}U fission chamber, operating in current mode. The plasma was heated with Neutral Beam Injection at a power level of about 14 MW, and the period of intense neutron emission was terminated by an influx of impurities.

3.2 14 MeV neutrons

For studies of mixed 14 and 2.5 MeV neutron fields, it is essential to use an active detector that permits a clear separation of 14 from 2.5 MeV neutrons. Several types of detector have been employed in triton burnup experiments, where the 14 MeV neutron yield is at most 2% of the 2.5 MeV yield. For this, liquid (DICKENS et al, 1987) and glass (COLESTOCK et al, 1979) scintillation detectors, fission detectors (JASSBY et al, 1987) (under special circumstances) and silicon surface-barrier detectors (CONROY et al, 1988) have all been used. Of these, the most satisfactory detector so far tested is the silicon diode. In this device, the (n,α) and (n,p) reactions induced by high energy neutrons provide large signals and the threshold energy of about 7 MeV ensures rejection of events due to 2.5 MeV neutrons. The use of this detector was pioneered at JET, using the remotely-sited electronics provided originally for counting mode operation of fission chambers. Subsequently, such detectors have been installed on other tokamaks using conventional electronics but with an amplifier located close to the detector. Due to the high energy threshold, the silicon detector is insensitive to gamma-radiation; it is unaffected by magnetic fields. There are two problems: firstly, radiation damage can be a serious concern, with a fluence limit (WEST, 1984) of about 10^{12} fast neutrons per cm^2, so that the detectors have to be replaced occasionally when operating with deuterium fuelled plasmas, and very frequently with high-yield deuterium-tritium plasmas; secondly, they can be used only in pulse-counting mode so the dynamic range is restricted.

Fig. 5 illustrates the use of a silicon diode for measurement of the weak 14 MeV neutron emission from triton burnup in the presence of the much stronger 2.5 MeV neutron emission. A time delay of the burnup signal relative to the 2.5 MeV source is clearly displayed. The time delay is a simple consequence of the t-D fusion reaction reaching its peak reactivity when the 1.0 MeV tritons have slowed down to an energy of about 180 keV; the reactivity dependence on triton energy is shown in fig. 6.

Fig. 7 shows the neutron emission for one of the first d-t plasma discharges (No. 26148) at JET, during which the neutron emission consisted almost entirely of 14 MeV neutrons, recorded with a silicon diode detector, as discussed above. The discharge conditions were similar to those for discharge 26087 (fig. 4) except that 2 MW of deuterium NBI were replaced by 2 MW of tritium NBI. Once more, the TRANSP simulation and reaction mode predictions are given.

3.3 Positioning of neutron detectors

An ideal position for neutron counters would be on the axis of symmetry of the tokamak, usually above or below the machine; more conveniently, the counters may be placed on the machine mid-plane, as close as possible and with an unobstructed view of a large fraction of the plasma volume. It is highly desirable that there be few, if any, massive obstructions between plasma and detector and that no changes to the dispositions of substantial nearby items of hardware should take place during the lifetime of the machine. In practice, these conditions are unlikely to be met, so that replication of the detectors is advised, on the grounds that most changes will affect one or more, but not all, of the detectors so that their occurrence can be noted and a knowledge of the overall calibration factors for the detectors can be maintained through cross-referencing, thereby reducing the need for frequent *in situ* calibrations.

3.4 *In situ* calibrations

The primary means of obtaining calibration factors for the neutron counters is through direct measurements performed with neutron sources that are conveniently small, in strength and size, placed at a large number of discrete positions inside the vacuum vessel so as to enable the volume emission of a plasma to be simulated. With the larger tokamaks (TFTR, JET, JT-60), where physical access into the vacuum vessel is relatively easy, rather extensive sets of measurements have been made. The ^{252}Cf radio-isotope source is the most convenient; the neutrons are emitted with the typical fission energy spectrum reaching up to 10 MeV but with a most probable energy of about 2 MeV.

Fig. 8 shows the variations in count-rate recorded in a fission counter as a ^{252}Cf neutron source was moved through 92 toroidal positions within the JT-60U tokamak (NISHITANI et al, 1992) . Based on such measurements, together with neutron transport calculations showing the equivalence of the energy spectra at the detector location for ^{252}Cf and deuterium plasma neutrons, an uncertainty of 11% was estimated for the resulting detection efficiency for plasma neutrons.

The calibration factors so obtained are only valid if it can be demonstrated that the ^{252}Cf energy spectrum is an acceptable substitute for D-D and D-T fusion sources. If it is not (see below), compact accelerator tubes with deuterium or tritium targets can be used instead. Such tubes have been used at TFTR

(NIESCHMIDT et al, 1985), and at JET (JARVIS et al, 1985); however, whilst the energy spectrum is now more appropriate, the accuracy of the measurement is somewhat degraded since the neutron emission from the tube (which will be quite massive) has to be fully characterized.

3.5 Modelling

In principle, it is feasible to obtain the calibration factor (emitted neutrons per recorded event) for neutron detectors entirely by computational means. The degree of reliability of the result depends on the care with which the tokamak, the detector and their environment have been modelled. This approach has been followed at JET to investigate the reasons for changes in the calibration factors that have occurred during the operational lifetime of the machine. It was found (LAUNDY and JARVIS, 1992) that, even with a relatively simple model and no free parameters, the neutron transport calculations reproduced, within 15% accuracy, the experimental calibration obtained at start-up of operations (i.e. before the major external diagnostic and additional heating components were installed). These calculations also showed that the ^{252}Cf energy spectrum gave a calibration factor that was about 10% higher than that for D-D neutrons. However, now that major external components have been added, it has been found experimentally that factor-of-four increases in the ^{252}Cf spectrum calibration factors have taken place and the neutron transport calculations show that the ^{252}Cf spectrum no longer gives an acceptable representation of D-D or D-T neutrons (up to factor-of-two over-estimates, depending on detector position). Clearly, direct calibrations of neutron counters should always be supplemented with numerical simulations.

3.6 Ion temperature measurements

One of the main reasons for operating tokamaks in deuterium is that the relatively easy measurement of the total neutron emission intensity during ohmic heating (and other conditions in which the ion energy distribution is expected to be maxwellian) provides a rather accurate measurement of the plasma ion temperature. As shown in fig. 3, the neutron yield scales with a relatively high power of the temperature, which can be determined to useful accuracy on the reasonable assumption of similar ion and electron temperature profiles, despite imprecise knowledge of the deuteron density. If the ion temperature is available, e.g. from neutron spectrometry (as discussed in section

6) or, for moderate-density plasmas, from neutral particle analysis (CORTI et al, 1986), then the neutron yield measurement can be used instead to derive the deuterium density or, more conveniently, the ratio of the deuterium to electron densities, n_d/n_e. Fig. 9 shows a comparison of ion temperature determinations from NPA and neutron yield measurements, based on the deduction from visible bremsstrahlung measurements that $n_d/n_e = 0.75$.

3.7 Operational experience

For tokamaks in which low-current ohmic heating is used, limiting the ion temperature to about 1 keV, a factor of two uncertainty in the absolute yield measurements leads to an estimate of the ion temperature with acceptable accuracy. For the larger tokamaks, with higher ion temperatures, the measurement accuracy needs to be as high as possible; in practice, better than 15% accuracy from *in situ* measurements has been claimed at TFTR (HENDEL and JASSBY, 1990), JT-60 (NISHITANI et al, 1992) and JET (JARVIS et al, 1985). A good account of the operational experience with neutron counters at TFTR, including the manner in which the *in situ* calibration is extrapolated to high neutron yields, is reported by HENDEL and JASSBY, (1990). For the reason explained in section 3.5, *in situ* source calibrations are no longer employed at JET, as the activation methods are considered to be more reliable.

4. TIME-INTEGRATED NEUTRON EMISSION

The use of neutron activation methods for determining the neutron fluence at the measuring point has a long history in neutron metrology, and methods have been developed that permit the full energy spectrum to be deduced for neutron energies ranging from thermal up to 20 MeV. Tokamak applications are less ambitious, since the interesting neutron energies are the nearly monoenergetic groups at 2.5 and 14 MeV. Nevertheless, the multi-foil analysis method constitutes a valuable test of the neutron transport methodology (PILLON et al, 1990).

The basic procedure followed for activation measurements is straightforward: a small sample of a suitable material is placed close to the tokamak plasma, with as little intervening material as possible. After one or more discharges, depending on the decay half-life of the chosen activation product, the sample is removed for measurement of the residual activity of the radionuclide of interest. From a

knowledge of the decay properties, the number of nuclei activated during the discharge is obtained. In order to convert this result into a measure of the total number of neutrons emitted from the plasma, it is necessary to rely on a calculation involving the known geometry of the tokamak relative to the sample position. For a relatively open tokamak and with the sample placed within the inner envelope of the toroidal field coils, the effect of neutron scattering on the high energy portion of the energy spectrum at the target can be ignored and the calculation can be performed analytically. Measurements falling into this category (ZANKL et al, 1981) have been performed at PLT using an indium sample, which is undoubtedly the best gamma-ray analysis material for measuring D-D neutrons. The result was used to obtain a calibration for the time-resolved neutron counters to an accuracy of ±30%. Similar measurements using copper, with its 12 MeV (n,2n) reaction threshold, permitted the 14 MeV neutrons from triton burnup to be detected in the presence of the far stronger fluxes of 2.5 MeV neutrons (COLESTOCK et al, 1979). Massive copper samples can be used (BATISTONI et al, 1987) when very low 14 MeV neutron yields have to be investigated, but self-shielding calculations are then necessary.

A practical difficulty which arises on the larger tokamaks is the need to position and remove the samples automatically; pneumatically operated sample transfer systems are employed, using polythene capsules. Both TFTR and JET have multiple irradiation position capability, while at JT-60 a single position is installed (NISHITANI, 1993). Since, for these machines, there is likely to be a significant amount of structural material between the sample and the plasma, it becomes essential to perform full neutron transport calculations to obtain the response coefficients for the materials of interest. The deployment of irradiation positions around the plasma at JET is shown in fig. 10; it is possible to obtain measurements for irradiation positions above and below the plasma median plane so that by averaging results from vertically opposed pairs of irradiation positions, any vertical displacement of the plasma position can be taken into account automatically. Fortuitously, if the irradiation positions are located at somewhat larger major radii than that of the plasma, then small shifts of plasma radial position also have little effect. For most geometries, the modelling problem is complex and it is highly desirable to obtain as many checks and cross-references between alternative materials and irradiation positions as possible. At JET, where two wholly independent neutron transport codes have been applied to the problem, MCNP (1982) and FURNACE (VERSCHUUR, 1984), experience has shown that the modelling difficulties are easily under-estimated and that the

samples must be placed as close as possible to the plasma, preferably inside the vacuum vessel within a relatively thin-walled irradiation tube.

Work at JET has demonstrated (JARVIS et al, 1991a) that the choice of indium for the activation material gives excellent results with d-d neutrons, although it is not practicable to make measurements for each and every discharge. This can be achieved, however, by using the delayed neutron counting technique (D'HONDT et al, 1986) with thorium samples. A fission reactor (the Belgian CEN/SCK BR-I research reactor) was used for determining the detection efficiency of the neutron counters to about 1% accuracy and, at the same time, the thorium cross-sections were normalized to the standard uranium cross-sections. The delayed neutron method gives more accurate results for the measured neutron fluences than does the use of indium, with agreement to within 3%; the calculation and modelling uncertainties for the response coefficients raises the uncertainty for the total yield estimates to ± 7%, at best.

For 14 MeV neutron measurements, the copper reaction is most frequently employed because of its high sensitivity. Other dosimetry materials, such as iron and aluminium, can also be used. All give nearly equivalent results. However, all have rather long decay half-lives and are unsuitable for repetitive use. Routine measurements are best performed using silicon (SADLER et al, 1990b), as this offers a decay half-life of only 2.2 minutes, so that the sample can be recycled between discharges if the discharge frequency is modest (< 4 per hour at JET). Silicon is not a dosimetry standard and reaction cross-sections are but poorly known, with only one precise measurement at 14.7 MeV; however, work at JET has shown that the excitation function, based on nuclear model calculations, that is provided in the European Fusion File (EFF, 1985) gives results that are in good agreement with those based on the use of copper.

In Table IV, we list some of the materials that have been applied to the measurement of D-D or D-T neutron yields at various tokamaks, together with brief comments on their important features. The threshold energy should be as high as possible to avoid unnecessary sensitivity to scattered neutrons but should not be too close to 2.5 or 14 MeV, otherwise the induced activation becomes highly sensitive to elastic scattering of neutrons by structures near to the measurement position, with a consequential need for considerable accuracy in modelling the geometry for response coefficient calculations. This point must be borne in mind when considering proposals (e.g. SMITHERS et al, 1988) for

obtaining a sensitive measure of the width of neutron energy distributions (to determine the ion temperature) by employing activation reactions that have excitation curves that rise rapidly throughout the energy spread of the fusion neutron spectrum.

The JET activation system has been extensively exploited. It was designed primarily for calibration purposes and, consequently, intermittent use. However, the development of the delayed neutron counting method and the discovery of the virtues of the silicon reaction, have permitted the time-integrated 2.5 and 14 MeV neutron yields to be obtained routinely, with data being stored along with the main JET Pulse File. Calibrations of the fission chamber data are therefore available for all interesting discharges, with no need for possibly dubious extrapolations. In fact, as shown in fig. 11, these activation measurements have been used to demonstrate that fission chamber responses do vary linearly with neutron intensity, to within measurement accuracy. It is also possible to monitor the neutron production from the reactions of fast ions with light impurities that are a feature of high power ICRF heated discharges.

Finally, nuclear emulsions (BAETZNER et al, 1990) and CR39 plastic films (MURPHY and STRACHAN, 1985) have both been used for low neutron fluence applications, the latter being particularly suitable for Health Physics purposes.

Table IV. Materials used for activation measurements in tokamaks

Reaction	Reaction Threshold (MeV)	Half-Life	Comments
		D-D neutrons	
$^{58}Ni(n,p)^{58}Co$	1.0	70.82 day	Major constituent in vacuum vessel materials.
$^{64}Zn(n,p)^{64}Cu$	1.8	12.70 hr	Questionable cross-section data. Rather high threshold energy. Avoid.
$^{115}In(n,n')^{115m}In$	0.5	4.486 hr	Good reaction for tokamak applications.
$^{232}Th(n,f)F.P.$	1.2	1 min	Most convenient. Normalize cross-sections to ^{238}U. Ideal for repetitive measurements.
$^{238}U(n,f)F.P.$	1.0	1 min	Inconvenient due to residual ^{235}U content.
		D-T neutrons	
$^{27}Al(n,p)^{27}Mg$	2.6	9.458 min	Low threshold energy.
$^{28}Si(n,p)^{28}Al$	5.0	2.25 min	Sparse cross-section data. Ideal for repetitive measurements.
$^{56}Fe(n,p)^{56}Mn$	4.5	2.577 hr	Magnetic material.
$^{63}Cu(n,2n)^{62}Cu$	10.9	9.74 min	Large cross-section. Interference from ^{64}Cu decays.

5. NEUTRON EMISSION PROFILES

The main function of a neutron profile monitor is to determine the (local) neutron emissivity over a complete poloidal section of the plasma from line-integrated measurements recorded by neutron detectors viewing the plasma along a large number chords (lines-of-sight) through the plasma. Each detector is required to function as a neutron spectrometer, if only to to distinguish neutrons that have undergone scattering events from those reaching the detector directly from the plasma. Because the absolute detection efficiency of the instrument should be known, the total instantaneous neutron yield from the tokamak can be obtained without need for recourse to activation measurements or in-vessel work for calibrating neutron yield monitors. Thus, a well-designed neutron profile monitor is potentially the most important of the range of neutron diagnostics; indeed, it combines many of the attributes of the others. However, it can never displace the other diagnostics, for the following reasons:

(i) as a neutron intensity monitor, it has a dynamic range that is likely to be limited to a few orders of magnitude,

(ii) achievement of an accurate (better than 10%) absolute global neutron detection efficiency for the instrument is a difficult task, so the profile monitor may supplement but cannot be considered an alternative to the calibration techniques discussed earlier,

(iii) it is impractical to provide sufficiently good energy resolution to fulfil the requirements of high resolution spectrometry.

The only tokamaks that presently have installed neutron profile monitors are TFTR and JET; these two monitors utilize entirely different detectors, as appropriate to the different geometrical arrangements and consequential problems. Both instruments will be described briefly.

5.1 The TFTR multi-collimator array

The design of the TFTR vacuum vessel was strongly influenced by the needs of the planned diagnostic instrumentation (in contrast to the situation at JET). The TFTR profile monitor, or multi-collimator array (ROQUEMORE et al, 1990), shown in fig. 12, comprises 10 vertical collimators, each providing lines-of-sight through the plasma that enter and leave the vacuum vessel through recessed thin vacuum windows so positioned as to be well outside the envelope of the main vacuum vessel; as a result, the scattering of neutrons into the lines-of-sight of the detectors is minimized. Since the detected flux of scattered neutrons is very small, it is not necessary to employ neutron detectors possessing good energy resolution in order to discriminate between virgin neutrons coming directly from the plasma against a background of neutrons that have lost energy as a result of scattering events. The TFTR plasmas are circular, so that a single viewing array is sufficient.

An attractive feature of the TFTR multi-collimator array is that it is provided with two large detector regions in which a variety of different detector types can be investigated. The detector selected for D-D neutrons (JOHNSON, 1992) is NE451, a derivative of the Hornyak button (HORNYAK,1952), utilising an arrangement of concentric rings of ZnS(Ag) scintillator crystals and clear plastic. The main advantage of NE451 is its insensitivity to gamma-radiation. The signal

amplitude spectrum from monoenergetic neutrons striking one of these detectors falls monotonically with pulse-height, and events due to 2.5 MeV neutrons are not intrinsically distinguishable from those due to 14 MeV neutrons. However, the signal rate due to 14 MeV neutrons from triton burnup is generally negligible in comparison with the D-D signal rate. The NE451 detector is suitable for D-T operation although the detection efficiency is likely to be rather too high; one proposed solution (ROQUEMORE and JOHNSON, 1992) to this latter problem is to image the scintillator onto the phototube in such a way that an adjustable iris can select a greater or smaller number of scintillator rings, as desired. Additionally, helium proportional counters are being tested (McCAULEY and STRACHAN, 1992).

5.2 The JET neutron profile monitor

Access for major diagnostic instrumentation on JET is limited mainly to two small vertical ports and a large horizontal port on each octant of the vacuum vessel. In order to view the whole of the plasma from either location, it is necessary to use a fan-like array of lines-of-sight, as illustrated in fig. 13. As appropriate for a machine with non-circular plasmas, two cameras are provided (ADAMS et al, 1993), one viewing downwards (the vertical camera) and the other from the side (the horizontal camera). The vertical camera has 9 channels (lines-of-sight); of these, only 3 view the inside of the lower vertical port and thereby benefit from a limited measure of protection against neutron backscattering. The horizontal camera possesses 10 channels, all of which view the central column of the machine. Thus, at JET, all of the detectors view the vessel walls and the separation of wall-scattered from virgin neutrons is vital. This can only be accomplished through energy discrimination. A hydrogenous scintillator, such as the conventional fast plastic NE102, could be suitable. However, the high efficiencies required for the study of low yield D-D plasmas necessitate the use of large scintillator volumes; unfortunately, large volume detectors are gamma-radiation sensitive. It therefore becomes necessary to distinguish gamma-ray induced events from neutron induced events; the conventional solution to this task is to use NE213 liquid scintillators (KNOLL, 1989) which permit n/γ discrimination on the basis of pulse shape analysis. This depends on the fact that, although the pulse forms are rather similar, the recoil proton from a neutron interaction is heavily ionizing and produces a number of rather long-lived excited atoms that are not produced by the weakly ionizing fast electron from a gamma-ray induced reaction. The Link Pulse-Shape Discriminator (LINK) is a

compact unit which simultaneously permits neutrons to be separated from gamma-rays and provides the necessary energy discrimination which, for D-D neutrons, is used to select proton recoil events falling in the neutron energy band from 2.0 to 3.5 MeV. It simultaneously selects gamma-rays with energies falling in the band 0.6 to 1.2 MeV. Thus, rather inadvertently, the neutron profile monitor also performs as an embryonic gamma-ray profile monitor, as will be illustrated below. In a recent upgrade, the profile monitor was equipped with two Pulse Shape Discriminator units per channel, to permit the D-T neutrons to be recorded simultaneously with D-D neutrons; the energy band used for D-T neutrons was from 7 to 17 MeV.

Typical neutron emission profiles for a deuterium discharge are illustrated in fig. 14, where the line-integrated signals for the 19 channels are compared with predictions from the TRANSP code. The full power of the tomographic method (GRANETZ and SMEULDERS, 1988 and MARCUS et al, 1991) is demonstrated by comparing, in fig. 15 (a) and (b), the 2-D emissivity plots taken just before and just after a major sawtooth crash; the flattening of the emission profile is obvious. In these examples, the curves of constant neutron emissivity lie very close to the magnetic flux surfaces, i.e. the emission shows nearly circular symmetry about the axis of the plasma.

Fast ion velocity distributions are not necessarily isotropic; this is detectable with neutral beam injected ions and is prominant for ions accelerated to high energies by ICRF heating as this preferentially increases the component of velocity normal to the toroidal magnetic field lines. In such cases, the magnetic flux surfaces can no longer be assumed to be contours of constant neutron (and gamma-ray) emission strength. An example of this is given in fig. 16, which shows the contour plots of gamma-ray emissivity (HOWARTH, 1993) for an ICRF-heated discharge in which a strong population of fast ^{3}He ions is generated; these ions undergo nuclear reactions with ^{9}Be impurity ions, resulting in the emission of characteristic gamma-rays and neutrons with energies of up to nearly 10 MeV. For the discharge shown, the ICRF resonance layer was positioned at the plasma axis, yet the fast particle orbits are confined to the low field side (larger major radius) of the plasma axis. This is the expected behaviour for trapped fast ions generated by ICRF heating.

With little more than an exchange of detectors, the JET profile monitor has also been used for measurements (BRUSATI et al, 1992) of the bremsstrahlung

radiation emitted by fast electrons generated during investigations with the Lower Hybrid Current Drive system. The current profile is diagnosed through observations of the fast-electron bremsstrahlung with energies up to 300 keV, using CsI/photodiodes.

The existing neutron profile monitor is at present being upgraded to provide improved radiation shielding (for D-T operation), remotely adjustable collimation (a choice of two aperture sizes), and to make provision for three in-line detectors within each collimation channel (a CsI/photodiode for fast-electron bremsstrahlung detection, an NE213 scintillator for D-D neutrons and low intensity D-T neutrons, and a small plastic scintillator for high intensity D-T neutrons). The number of channels and their viewing directions will remain unchanged.

6. NEUTRON SPECTROMETRY

The original motivation for measuring the energy spectra of neutrons emitted from fusion plasmas was the determination of the ion temperature (LEHNER and POHL, 1967) from ohmically heated discharges. In order to measure the thermal broadening, it is necessary that a high resolution neutron spectrometer be employed. Normally, the spectrometer response function can be approximated by a gaussian with *fwhm* (R) that defines the effective energy resolution. As described in section 2.4, the neutron energy spectrum from thermonuclear plasmas is accurately represented by a gaussian whose *fwhm* (F) is defined by the thermal broadening. To be useful, the energy resolution offered by the spectrometer needs to be rather less than the thermal broadening ; ideally, $R \leq 0.5$ F. Thus, for an ion temperature of 4 keV, the spectrometer resolution should be better than 3.3% for a deuterium plasma and 1.3% for a deuterium-tritium plasma. Such values are achievable, but only by sacrificing detector efficiency which must be high enough to permit a useful spectrum (containing between 200 and 1000 events) to be obtained in the required measurement time (of order of one second). Clearly, a difficult compromise has to be made between resolution and efficiency.

Since neutron spectrometers are generally low efficiency devices, it is important to know the relationship between the number of useful events (N) in the energy spectrum and the resulting uncertainty in temperature estimate for plasmas in thermal equilibrium. This relationship is easily obtained in the case of a

spectrometer with gaussian response function, of *fwhm R*. Assuming *R* to have been determined precisely by experiment or modelling ($\delta R=0$), then (JARVIS,1983)

$$N = 2\left(\frac{T_i}{\delta T_i}\right)^2\left[1+\frac{R^2}{F^2}\right]^2,$$

where *F* is the *fwhm* of the neutron spectrum. As an example, when *R* is small, 200 counts will suffice to provide a temperature measurement to 10% accuracy. Caution is needed when using the above formula: it only applies for gaussian response functions. Should the response function consist of a very narrow, almost gaussian peak, but with a significant low energy tail (as in the case of the ^{3}He spectrometer, discussed below) then it will be found (GORINI, 1985) that an appreciably greater number of counts will be required in order to obtain the desired statistical accuracy for the temperature measurement; application of the above relationship will permit an *effective* energy resolution to be assigned to the spectrometer. More formally correct, the second moment of the response function should be used to define the energy resolution instead of the *fwhm* of the *effective* gaussian.

Owing to the strong increase of fusion reactivity with temperature, it is frequently assumed that temperatures determined with a neutron spectrometer that has a line-of-sight passing through the plasma centre will correspond mainly to central conditions; this is not entirely correct, although the necessary line-of-sight correction (LOUGHLIN, 1991) for optimum conditions is, typically, only 10%. In principle, neutron spectrometry can be employed for ion temperature profile measurements. This development is not appropriate for the present generation of tokamaks.

A variety of neutron detector types has been used for neutron spectrometry of tokamak plasmas; these include measurement of proton recoil tracks in nuclear emulsions (HUEBNER et al, 1985), the hydrogen spherical proportional chamber (HOENEN and BIEGER, 1987), the ubiquitous NE213 liquid scintillator proton recoil spectrometer and variants of thin foil proton recoil devices. None of these is suitable for high-resolution time-resolved spectrometry. Nevertheless, low-resolution spectrometers that cover a wide energy range may be very useful for indicating the presence of energetic neutrons generated by ICRF-accelerated ions reacting with light impurity species.

The only high resolution neutron spectrometers which perform satisfactorily with deuterium plasmas are the commercial ^{3}He ionization spectrometer (MODEL FNS-1), and the time-of-flight spectrometer as developed for use at JET (ELEVANT et al, 1991). There appears to be little scope for development of improved instruments for 2.5 MeV neutrons. There is, on the other hand, considerable scope for the innovative design of spectrometers for use with 14 MeV neutrons. Only two such instruments have so far been constructed (both for deployment at JET); these are the highly efficient tandem-radiator proton recoil instrument (HAWKES et al, 1986), and the high-resolution associated-particle time-of-flight spectrometer (GROSSHOEG et al, 1986). Another possibility that has been discussed in the literature is the use of magnetic analysis of recoil protons (KALLNE and ENGE, 1992) .

6.1 Deuterium plasmas

The ^{3}He ionization neutron spectrometer was first used to good effect by STRACHAN et al, (1979) for investigations of hydrogen beam heated plasmas on PLT. It was then used for ohmic plasmas on Alcator-C deuterium plasmas in a definitive work by FISHER, 1983 and, subsequently, on TFTR by STRACHAN et al, (1988). These early measurements served to prove the principle but it was left to JET to demonstrate the practical value of the technique (JARVIS et al, 1986). Fig. 17 shows typical experimental neutron energy spectra, and compares them with computed spectra obtained by folding a gaussian with the response function of the spectrometer, using the *fwhm* of the gaussian as the fitting parameter, and the gaussians (shown as dotted lines) from which the temperatures (after line-of-sight correction) are finally deduced. The combination of such temperature measurements and the total neutron emission strength gave the first warning that the n_d/n_e density ratio in JET deuterium plasmas bounded by carbon limiters falls with increasing temperature and is typically 0.5 for ohmic discharges, as shown in fig. 18. Higher values of n_d/n_e are obtained with beryllium limiters.

The ^{3}He spectrometer that is universally employed is a commercial spectrometer intended for use with *circa* 1 MeV neutrons. It provides an effective energy resolution of about 3% for 2.5 MeV neutrons; unfortunately, it is unusable in the presence of neutrons with energies in excess of 4 MeV because the proton from the n(^{3}He,p)t reaction has too great a recoil energy to be stopped by the working gas before reaching the wall and therefore contributes a signal indistinguishable

from that due to a lower energy neutron. The charge collection time is rather long, imposing a severe count-rate restriction, so that the minimum counting time required for the accumulation of a statistically acceptable spectrum is at least 2.5 seconds at constant count-rate. These limitations prevent the ^{3}He spectrometer from performing effectively in most high performance discharges at JET, not only because the neutron emission duration is less than 2 seconds but also because ICRF heating frequently generates a high energy (>4 MeV) component to the neutron emission. Notwithstanding these disadvantages, the ^{3}He spectrometer is likely to continue to be the favoured instrument in most laboratories because of its low cost and compact size; it has to be provided with suitable protection against background neutron and gamma-radiation but this can be achieved within a modest space envelope (about 1 metre thick shielding walls) so that the instrument can be placed very near the tokamak. Another reason for the ^{3}He spectrometer having a useful role to play even when it has apparently been superseded by other instruments is because its compact size facilitates transportability, permitting its detailed characterization at an accelerator laboratory for use as a neutron flux intensity and energy resolution standard against which the other instruments, for which such characterization is not feasible, can be compared. The detector response as a function of energy has been reduced to a convenient parametric form for use with spectrum unfolding codes (LOUGHLIN et al, 1990).

Because of the disadvantages mentioned above, the use of the ^{3}He spectrometer has fallen out of favour at JET. Instead, a time-of-flight neutron spectrometer (ELEVANT, 1992) (fig. 19) is now employed in which the neutrons pass through a scintillator placed in the line-of-sight; a few scatter towards a large bank of neutron detectors placed at a distance of about 2 metres and the flight times of the neutrons are measured. This information, together with a knowledge of the geometry of the arrangement, permits the neutron energy spectrum to be determined. The present instrument, an upgrade of a prototype time-of-flight spectrometer (ELEVANT, 1991), now provides an energy resolution of 4.6% and an efficiency of 5×10^{-2} counts per unit flux, (i.e. counts/n.cm^{-2} or just cm^2) that exceeds that of the ^{3}He spectrometer; furthermore, the count-rate limitation is much higher and there is no comparable difficulty from the high energy neutron contribution. The major disadvantage of the time-of-flight approach is the need for a large experimental area that is well screened from background neutron and gamma-radiation; at JET, this is resolved by placing the instrument in a Roof Laboratory, directly above the tokamak, with a 2-metre thick concrete floor.

Fig. 20 illustrates the quality of the neutron energy spectra that can be obtained with the time-of-flight spectrometer. The plasma discharge illustrated was heated with deuterium neutral beams only, so that the neutron spectrum comprises a superposition of contributions from thermal, beam-plasma and beam-beam fusion reactions. This complicates the interpretation considerably. The information that can be derived directly from analysis of such spectra depends on the plasma conditions. Under favourable circumstances (ion temperatures below 10 keV), it is possible to determine both the deuterium temperature and density independently of other diagnostic information; for less favourable circumstances, it is only possible to determine one of these two quantities, given a separate estimate for the other. In both cases, it is necessary to compute the shape of the beam-plasma neutron energy spectrum, based on a knowledge of the properties of the neutral beam injection system. A detailed discussion of neutron spectrum analysis for beam-heated plasmas may be found in OLSSON, (1993). The possible consequences of applying high ICRF heating powers is illustrated in fig. 21, which shows energy spectra obtained with the time-of-flight spectrometer for two similar discharges with combined NBI and ICRF heating; the difference is that the ICRF only generates a fast proton population for one of the discharges, as demonstrated by the presence of the very energetic neutrons from p-^{9}Be nuclear reactions.

6.2 Plans for measurements with deuterium-tritium plasmas

The tandem-radiator 14 MeV neutron spectrometer is based on a design developed in Korea (KANG and CHUNG, 1975) for studying fission reactor neutron emission. For application at JET, the spectrometer was originally conceived as being a relatively compact instrument that could be provided with a local radiation shield for installation inside the Torus Hall, near to the tokamak for optimum detection efficiency. This plan was eventually abandoned when a viewing location outside the main biological shield wall became available. The instrument, illustrated in fig. 22, utilizes an annular collimator and is based on the nearly-forward scattering of protons from an annular thin foil, or radiator, of polythene into a silicon diode detector placed on the axis of the collimator. The axial portion of the collimator (a "shadow bar") protects the diode from the direct flux of neutrons from the tokamak. Three pairs of radiator-detector combinations are provided for increased efficiency. The theoretical efficiency is 8×10^{-5} cm^2 and the resolution is 2.5%. The spectrometer has been partially tested at an accelerator facility but not yet at JET.

The associated-particle time-of-flight spectrometer (GROSSHOEG et al, 1986), shown in fig. 23, is a development of the 2.5 MeV time-of-flight spectrometer, intended to overcome the excessively high random counting rates between the in-line scattering detector and the scattered neutron detectors that will occur for high performance discharges. The scatterer is now a passive foil aligned unconventionally, with its surface parallel to the neutron beam. The bulk of the energy of the incident neutron is determined by detecting small-angle knock-on protons with silicon diode detectors and the residual energy carried off by the recoiling neutrons is measured by conventional time-of-flight methods. The spectrometer comprises two mirrored banks of detectors, both comprising 3 silicon diodes and 16 neutron detectors, with each of the three diodes placed in coincidence with all 16 neutron detectors. The overall efficiency is rather low at 10^{-5} cm^2 but the energy resolution is excellent at 1.1%. This spectrometer has been tested extensively in an accelerator laboratory but has yet to be proven at JET, where it will be located in the well-shielded Roof Laboratory. A desirable feature of this instrument is the placing of the plane of the scattering foil along the direction of incidence of the incoming neutrons; this permits the use of a very narrow collimation slit, with a considerable reduction in the flux of neutrons entering the Roof Laboratory.

One other spectrometer which should be mentioned is the silicon diode (ELEVANT, 1986); this offers an energy resolution of about 0.8% and an efficiency of about 10^{-4} cm^2. It has a limited counting rate capability, suffers from radiation damage, and should not be used for spectra which are broader than a few percent because the response function consists of a number of relatively narrow lines that should not be permitted to overlap when folded into a wide energy spectrum. Nevertheless, the silicon diode can be used as a reference standard in the manner suggested for the ^3He spectrometer.

In one respect, neutron spectrometry with D-T plasmas will be simpler than with D-D plasmas: the neutrons produced from reactions between ICRF-accelerated light ions and plasma impurity species will not be sufficiently energetic to interfere with the neutron spectrum from D-T fusion reactions and, moreover, their relative intensity will be at the percentage level. As a result, it will be easier to examine the fast deuteron or triton population associated with ICRF heating through the distortion of the 14 MeV neutron spectrum. A major challenge for neutron spectrometry with D-T plasmas will be to quantify the D-D and T-T fusion reaction rates in addition to the D-T rate; given this information, the

deuteron and triton densities in the plasma could be determined directly. Such measurements may be possible, provided a line-of-sight that does not intercept any substantial vacuum vessel components can be established through the plasma.

6.3 Summary

Table V (below) contains a summary of the D-D neutron spectrometer types that have been used at JET, along with those currently being implemented for D-T operation.

Table V. Properties of Neutron Spectrometers in use at JET

Spectrometer type	Efficiency (cm^2)	Energy resolution (*fwhm*, $\delta E/E\%$)	Physical dimensions whl (m^3)
	D-D plasmas		
^3He spectrometer	$1\ 10^{-2}$	3	Small
Time-of-flight	$5\ 10^{-2}$	4.9	4 4 2
	D-T plasmas		
Proton recoil	$8\ 10^{-5}$	2.5	0.4 1 2
Associated-particle, time-of-flight	$1.4\ 10^{-5}$	1.1	4 4 2
Silicon diode	$1.3\ 10^{-4}$	0.8	Small (2 mm thick)

Neglecting surrounding shielding.

7. CONCLUSIONS

With the advent of the larger tokamaks, neutron diagnostics have begun to play a major role in plasma diagnostics. Not only do they provide essential information concerning fusion reaction rates but they also provide a new and powerful means of determining various properties of particle transport (JARVIS, 1991b). With the move towards even larger machines, such as ITER (MUKHOVATOV et al, 1990), their role is likely to become even more important because the problems of quasi-continuous operation at high levels of neutron and gamma-ray backgrounds will make many of the more conventional techniques decidedly unattractive. Despite the anticipated two order-of-magnitude increase in fusion power in ITER over the best achievable in present-

day machines, the neutron diagnostics need not be very different from those described in this review, since the greater size of ITER leads to an increase in the neutron flux at external measuring points of only one order-of-magnitude.

ACKNOWLEDGEMENTS

The author is very grateful to past and present members of the JET Neutron Diagnostics Group who have all contributed to the topics covered in this paper and, in particular, to those who have provided previously unpublished material. The unique contribution from the staff at Princeton University who, while working on PLT, pioneered the early measurements and effectively defined the nature of the instrumentation that was to be constructed later, is also acknowledged.

REFERENCES

ADAMS, J.M., JARVIS, O.N., SADLER, G.J., SYME, D.B. and WATKINS, N. The JET Neutron Emission Profile Monitor, (to be published in *Nucl. Instrum. and Meth. in Phys. Res.*), (1993) and *JET Joint Undertaking Preprint* JET-P(92)27.

BAETZNER, R., HUBNER, K., INGROSSO, L., WAGNER, R., BOMBA, B. et al. Absolute determination of high neutron yields for ASDEX, *Proc. of the 17th EPS Conference on Controlled Fusion and Plasma Heating*, Amsterdam, 1990. *Europhysics Conference Abstracts* **14B** (1990) 1520.

BATISTONI, P., MARTONE, M., PILLON, M., PODDA, S. and RAPISARDA, M. *Nuclear Fusion* **27** (1987) 1040.

BOSCH, H-S. Fusion Products Bibliography, Version 3.0. (August 1991). Max-Planck Institut fuer Plasma Physik, Association EURATOM-IPP, D-8046 Garching, West Germany.

BOSCH, H.-S. and HALE, G.M. *Nuclear Fusion* **32** (1992) 611.

BROWN, R.E., JARMIE, N. and HALE, G.M. *Phys.Rev. C* **35** (1987) 1999 and **36** (1987) 1220.

BROWN, R.E. and JARMIE, N. *Phys. Rev. C* **41** (1990) 1391.

BRUSATI, M., BARTLETT, D., BOSIA, G., EKEDAHL, A., FROISSARD, P. et al, Lower Current Drive Experiments on JET, Submitted to *Nuclear Fusion* (1992) and *JET Joint Undertaking Preprint* JET-P(91)45.

BRYSK, H. *Plasma Physics* **15** (1973) 611.

COLESTOCK, P., STRACHAN, J.D., ULRICKSON, M. and CHRIEN, R. *Phys. Rev. Letters* **43** (1979) 768.

CONROY, S., JARVIS, O.N., SADLER, G. and HUXTABLE, G.B. *Nuclear Fusion* **28** (1988) 2127.

CORDEY, J.G. and CORE, W. *Physics of Fluids* **17** (1974) 1626.

CORTI, S., BARBATO, E., BRACCO, G., BRUSATI, M., BURES, M., GONDHALEKAR, A. et al. T_i Profile Studies during ICRF Heating in JET, *13th European Physical Society Conference on Controlled Fusion and Plasma Heating*, Schliersee, April 1986. *Europhysics Conference Abstracts* **10C** (1986) 109.

D'HONDT, P., DE LEEUW, S., MENIL, R. and BORTELS, Y. Delayed Neutron Counting System for JET Plasma Neutron Yields Diagnostic, Centre d'Etude de L'Energie Nucleaire/Studiecentrum voor Kernenergie (1986),*CEN/SCK Report* No. 528007/510.

DICKENS, J.K. et al. *Fusion Technology* **12** (1987) 270.

EFF. European Fusion File, see Index of JEF-1 Nuclear data Library, NEA Data-Bank, July 1985.

ELEVANT, T., HENDEL, H.W., NIESCHMIDT, E.B. and SAMUELSON, L.E. *Rev.Sci.Instrum.* **57** (1986) 1763.

ELEVANT, T.E. et al. *Nucl. Instrum. Methods.* **A306** (1991) 331.

ELEVANT, T., VAN BELLE, P., GROSSHOEG, G. et al. *Rev. Sci. Instrum.* **63** (1992) 4586.

ENGLAND, A.C., HENDEL H.W. and NIESCHMIDT, E.B. *Rev.Sci.Instrum.* **57** (1986) 1754.

FISHER, W.A., CHEN, S.H., GWINN D. and PARKER, R.R. *Phys. Rev.* **A28** (1983) 3121.

GOLDSTON, R.J., McCUNE, D.C., TOWNER, H.H. et al. *J.Comput.Phys.* **43** (1981) 61.

GORINI, G., HONE, M., JARVIS, O. N. et al. Ion temperature measurement in JET using neutron spectra. *Course and Workshop on Basic Physical Processes of Toroidal Plasmas*, Varenna, 1985.

GRANATSTEIN, V.L. and COLESTOCK, P.L., eds. *Wave Heating and Current Drive in Plasmas*, Gordon and Breach, New York (1985).

GRANETZ, R.S. and SMEULDERS, P., *Nuclear Fusion* **28** (1988) 457.

GROSSHOEG, G., ARONSSON, D., BEIMER, K.-H. et al. *Nucl. Instrum. and Meth. in Phys. Res.* **A249** (1986) 468.

HAWKES, N.P., van BELLE, P., HONE, M., JARVIS, O.N., LOUGHLIN, M.J. and SWINHOE, M.T. *To be submitted to Nucl. Instrum. and Meth. in Phys. Res. (1993),* and *JET Joint Undertaking Preprint* JET-P(93)**.

HEIDBRINK, W.W. *Rev. Sci. Instrum.* **57** (1986) 1769.

HENDEL, H.W. and JASSBY, D.L. *Nuclear Science and Engineering* **106** (1990) 114.

HOENEN, F. and BIEGER, W. *Nucl. Instrum. and Methods in Phys. Res.* **A259** (1987) 529.

HORNYAK, W.F. *Rev.Sci.Instrum.* **23** (1952) 264.

HOWARTH, P.J.A. (priv. comm., 1993).

HUEBNER, K., BAETZNER, R., HINSCH, H., RAPP, H., WURZ, H. et al, Neutron Production during Deuterium Injection in Deuterium Plasmas in ASDEX, *Proc. of the 12th European Conference on Controlled Fusion and Plasma Physics*, Budapest, 1985. *Europhysics Conference Abstracts* **9F** (1985) 231.

JARVIS, O.N. Neutron Detection Techniques for Plasma Diagnostics,*Course and Workshop in Diagnostics for Fusion Reactor Conditions*, Varenna, 1982. Brussels: Commission of the European Communities (1983), p.353.

JARVIS, O.N., KALLNE, J., SADLER, G., van BELLE, P. et al. Further calibrations of the time-resolved neutron yield monitor (KN1), (1985). *JET Joint Undertking Internal Report JET-IR(85)06.*

JARVIS, O.N., GORINI, G., HONE, M. et al. *Rev. Sci. Instrum.* **57** (1986) 1717.

JARVIS, O.N., GORINI, G., KALLNE, J., MERLO, V., SADLER, G. and van BELLE, P.,*Nuclear Fusion 27 (1987) 1755.*

JARVIS, O.N., SADLER, G. and THOMPSON, J.L. *Nuclear Fusion* **28** (1988) 1981.

JARVIS, O.N., CLIPSHAM, E., HONE, M. et al. *Fusion Technology* **20** (1991a) 265.

JARVIS, O.N. Neutron and gamma-ray diagnostics. *Diagnostics for Contemporary Fusion Experiments*, International School of Plasma Physics Piero Caldirola, Societa Italiana di Fisica, Bologna, Italy (1991b), p.541.

JARVIS, O.N. *Rev. Sci. Instrum.* **63** (1992) 4511.

JASSBY, D.L., HENDEL, H.W., BARNES, C.W. et al. Fission Detector determination of d-d Triton Burnup Fraction in Beam-Heated TFTR plasmas", *Proc.14th European Conf. Controlled Fusion and Plasma Physics*, Madrid, Spain, 1987. Europhysics Conference Abstracts **11D** (1987) 1264.

JET TEAM, *Nuclear Fusion* **32** (1992) 187.

JOHNSON, L.C. *Rev. Sci. Instrum.* **63** (1992) 4517.

KALLNE, J. and ENGE, H. *Nucl. Instrum. Meth. in Phys. Res.* **A311** (1992) 595.

KANG, H.D. and CHUNG, M.K. *J.Korean Phys.Soc.* **8** (1975) 9.

KNOEPFEL, H. and SPONG, D.A. *Nuclear Fusion* **19** (1979) 785.

KNOLL, G.F. *Radiation Detection and Measurement* (Wiley, New York, 1989).

LANE, A.M. and THOMAS, R.G. *Reviews of Modern Physics* **30** (1958) 257.

LAUNDY, B.J. and JARVIS, O.N. Numerical study of the calibration factors for the neutron counters in use at the Joint European Torus, *JET Joint Undertaking Preprint JET-P(92)60.* Submitted to *Fusion Technology* (1992).

LEHNER, G. and POHL, F. *Z.Phys.* **207** (1967) 83.

LINK ANALYTICAL LTD., High Wycombe, Bucks., England.

LOUGHLIN, M.J., ADAMS, J.M. and SADLER, G.J. *Nucl. Instrum. and Methods in Phys, Res. A* **294** (1990) 606.

LOUGHLIN, M.J. Profile Effects on Ion Temperature Measurements derived from Neutron Spectrometry, *Diagnostics for Contemporary Fusion Experiments*, ISPP-9 Piero Caldirola, International School of Plasma Physics Piero Caldirola, Societa Italiana di Fisica, Bologna, Italy (1991), p.1043.

MARCUS, F.B., ADAMS, J.M., CHEETHAM, A.D. et al.,

Plasma Physics and Controlled Fusion **33** (1991) 277.

MARCUS, F.B., ADAMS, J.M., BALET, B., BOND, D.S., et al.,*Submitted to Nuclear Fusion (1993)* and *JET Joint Undertaking Preprint* JET-P(93)**.

McCAULEY, J. S. and STRACHAN, J.D. *Rev.Sci. Instrum.* **63** (1992) 4536.

MCNP - A General Purpose Monte-Carlo Code for Neutron and Photon transport, *Los Alamos National Laboratory Report* LA-7396-M Rev., Version 2B, (1982).

MODEL FNS-1, manufactured by Jordan Valley Applied Radiation Ltd (Migdal Hamaek), P.O. Box 103, Israel 10550.

MUKHOVATOV, V., HOPMAN, H., YAMAMOTO, S. et al, ITER Diagnostics, *ITER Documentation Series No.33*, IAEA Vienna (1990).

MURPHY, T.J. and STRACHAN, J.D. *Nuclear Fusion* **25** (1985) 383.

NIESCHMIDT, E.B., ENGLAND, A.C., HENDEL, H.W. et al. Rev. Sci. Instrum. **56** (1985) 1084.

NISHITANI, T., TAKEUCHI, H., KONDOH, T. et al. *Rev. Sci. Instrum.* **63** (1992) 5270.

NISHITANI, T. (priv. comm., 1993).

OLSSON, M., VAN BELLE, P., CONROY, S., ELEVANT, T. and SADLER, G. *Plasma Physics and Controlled Fusion* **35** (1993) 179.

ORLINSKIJ, D.V. and MAGYAR, G. *Nuclear Fusion* **28** (1988) 611.

PILLON, M., JARVIS, O.N. and CONROY, S. Neutron energy spectrum determination near the surface of the JET vacuum vessel using the multifoil activation technique, *Fusion Engineering IEEE 13th Symposium*, Knoxville , Oct. 1989, New York, IEEE (1990), p160.

ROQUEMORE, A.L., CHOUNIARD, R.C., DIESSO, M. et al. *Rev. Sci. Instrum.* **61** (1990) 3163.

ROQUEMORE, A.L. and JOHNSON, L.C. *Rev.Sci.Instrum.* **63** (1992) 4539.

SADLER, G., ADAMS, J.M., ATTENBERGER, S. et al. D-D neutron production from JET plasmas, *Proc. 17th Europ. Conf. on Controlled Fusion and Plasma Heating*, Amsterdam, 1990. *Europhysics Conference Abstracts* **14B** (1990a) 1.

SADLER, G., JARVIS, O.N. and van BELLE, P. *Rev. Sci. Instrum.* **61** (1990b) 3175.

SLAUGHTER, D. *Rev.Sci.Instrum.* **57** (1986) 1751.

SMITHERS, R.K., GREENWOOD, L.R. and HENDEL, H. *Rev. Sci. Instrum.* **56** (1988) 1078.

STIX, T.H. *Nuclear Fusion* **15** (1975) 737.

STRACHAN, J.D. et al., *Nature* **279** (1979) 626.

STRACHAN, J.D., NISHITANI, T. and BARNES, C.W. *Rev. Sci. Instrum.* **59** (1988) 1732.

van BELLE , P. and SADLER, G. The computation of fusion product spectra from high temperature plasmas, *Basic and Advanced Diagnostic Techniques for Fusion Plasmas*, Varenna 1986. CEC Brussels, EUR 10797 EN, Vol. III (1987).

VERSCHUUR, K.A. FURNACE, A Toroidal Geometry Neutronic Program System; Method, Description and Users Manual.*Netherlands Energy Research Foundation Report* ECN-162 (1984).

WEST, D. Radiation damage to Si diode detectors by 14 MeV neutrons, *U.K.A.E.A. Report* AERE-R11481 (1984).

ZANKL, G., STRACHAN, J.D., LEWIS, R., PETTUS W. and SCHMOTZER, J. Nucl. Instrum. and Methods **185** (1981) 321.

FIGURES

Fig.1: The variation of the total cross-section with energy for the three neutron-producing fusion reactions. The (thermal) target particles are denoted by upper-case letters and the bombarding particles, or projectiles, by lower-case letters. The projectile energy is given in keV for the laboratory frame of reference.

Fig.2: The variation of the reactivity with plasma temperature for the three neutron-producing reactions. A Maxwellian ion energy distribution is assumed.

Fig.3: The variation of the exponent γ with plasma temperature for the D-D_n and D-T fusion reactivities when the plasma reactivity is described by the power dependence T_i^{γ}.

Fig.4: The time-dependence of the 2.5 MeV neutron emission for discharge number 26087; this is the highest d-d intensity yet achieved at JET . Discharge 26087 was one of a series preparatory to the first tritium discharges in JET (JET Team, 1992). The plasma was heated with 14 MW of deuterium NBI. The neutron emission as simulated with TRANSP is also shown, to indicate the relative rates due to thermal, beam-thermal and beam-beam fusion reactions.

Fig.5: The 2.5 MeV neutron emission is compared with the 14 MeV neutron emission from triton burnup reactions, as measured with a silicon diode, for JET discharge 26061. The time delay between the source fusion reactions (the 2.5 MeV neutron signal) and the resulting burnup signal is clearly exhibited.

Fig.6: The variation of the t-D reactivity, $\langle\sigma v\rangle$, with triton (laboratory) energy for a cold target. The peak at about 180 keV is reached after the tritons have been slowing down (from 1.0 MeV) for, typically, about 300 ms in a hot plasma.

Fig.7: The time-dependence of the 14 MeV neutron emission from JET discharge 26148, the record intensity obtained from any tokamak to date (JET Team, 1992). For this discharge, 2 MW of deuterium NBI was replaced by 2 MW of tritium NBI. The neutron production rates due to thermal, beam-thermal and beam-beam fusion reactions derived from a TRANSP simulation are shown. As for discharge No. 26087 (fig. 4), the period of intense neutron emission was terminated by an influx of impurities from the surrounding structures.

Fig.8: The dependence of neutron detector count-rate is shown as a function of toroidal position of a ^{252}Cf neutron point source in the JT-60U tokamak (from Nishitani et al., 1992). Integration of such data to simulate a plasma provides an accurate calibration of the detector response to deuterium plasma conditions. The predictions obtained with a neutron transport simulation are also shown.

Fig.9: Comparison of ion temperatures from Neutral Particle Analysis and neutron yield measurements for JET discharge number 3908, using the value of 0.75 for the dilution ratio n_d / n_e derived from visible bremsstrahlung measurements.

Fig.10: Showing a poloidal section through the JET tokamak to indicate the positions at which activation measurements may be obtained. There is mirror symmetry in the horizontal mid-plane.

Fig.11: Demonstrating the high degree of linearity between the time-integrated neutron emission recorded by the JET fission chambers, calibrated at very low yields, with that obtained from activation measurements. The duration of the main period of neutron emission was typically about 1 second. For neutron yields in excess of 10^{14}, the statistical uncertainty in each measurement is much smaller than the plotting symbol.

Fig.12: Elevation view of the TFTR multicollimator, showing the essential collimator components and the associated shielding (from Roquemore et al, 1990).

Fig.13: Illustrating the 19 lines-of-sight of the JET neutron profile monitor.

Fig.14: Neutron emission profiles for JET discharge No. 26087, taken at the moment of peak neutron emission. The line-integrated signals for each of the 19 channels are compared with predictions from the TRANSP code. (From Marcus et al., 1993).

Fig.15: Tomographic analysis provides the 2-D emissivity plots for JET discharge No. 26087 for two periods: (upper) just before the sawtooth crash at 12.35 seconds, and (lower) just after the crash. (From Marcus et al., 1993).

Fig.16: A contour plot of gamma-ray emissivity for an ICRF-heated discharge (JET discharge No. 23453) with resonance layer situated 16 cm from the plasma axis (Howarth et al., 1993). The gamma-rays are generated by nuclear interactions between fast ^{3}He ions and impurity ^{9}Be ions; there is an associated production of neutrons that has the same spatial origin. The positions of the magnetic flux surfaces are indicated. The fast ions possess a highly anisotropic velocity distribution and are trapped on the low field side of the resonance position.

Fig.17: Neutron energy spectra taken at JET with a ^{3}He ionization chamber spectrometer (Jarvis et al., 1986). The period of integration for these spectra was 5 sec. or longer. The data are fitted with a variable-width gaussian folded into the detector response function to obtain the most probable ion temperature; the deduced temperatures at the centre of the plasma are shown, after correction for line-of-sight averaging.

Fig.18: The variation of the dilution ratio n_d / n_e as a function of plasma temperature, for some ohmically heated deuterium discharges and two ICRF-heated discharges, with carbon limiters. The ion temperatures were derived from neutron spectra, as illustrated in fig 17, obtained using a ^{3}He ionization chamber spectrometer. (From Jarvis et al., 1987).

Fig.19: Photograph of the JET 2.5 MeV neutron time-of-flight spectrometer. The neutron beam is defined by a vertical collimator set into the floor, and pass through the scintillator placed close to the floor, on the axis of the 32-detector array.

Fig.20: Neutron energy spectra obtained with the JET 2.5 MeV neutron time-of-flight spectrometer for NBI-heated discharge No. 25432, to illustrate the high count-rate capability. Analysis (the fitted curves) permits the relative proportions of thermal to beam-plasma reaction rates to be determined, based on ion temperatures from X-ray spectroscopy. The first spectrum corresponds to beam-plasma reactions in a cold plasma; subsequent spectra show the ion temperature rising to apeak at about 18 keV, when thermal, beam-plasma and beam-beam reactions are of comparable magnitude; the final spectra show the rapid collapse of the temperature and neutron yield due to an uncontrolled influx of impurities. (From Elevant et al., 1992).

Fig.21: Neutron energy spectra obtained with the JET 2.5 MeV neutron time-of-flight spectrometer for two similar discharges with combined NBI and ICRF heating; in discharge No. 25190, the plasma conditions are such that the ICRF generates a fast proton population that produces high energy neutrons from interactions with ^{9}Be impurity ions. A random coincidence count-rate subtraction has been made.

Fig.22: Illustrating the principle of the JET tandem radiator spectrometer. The annular flux of neutrons passes through the three polythene foils; protons recoiling at small angles may be detected by the silicon diodes placed on the axis of symmetry of the instrument. The diodes are protected from the incident neutrons by means of a shadow bar set in the 2-m thick shield wall.

Fig.23: Illustrating the principle of the JET associated particle neutron time-of-flight spectrometer. Source neutrons enter vertically through the collimator (1); scattering occurs in the polyethylene foil (2). The recoil protons are detected in the 6 proton detectors (3) located inside the vacuum chamber and the associated scattered neutrons are recorded in coincidence in the two banks of 16 neutron detectors (4). (From Grosshoeg et al., 1987).

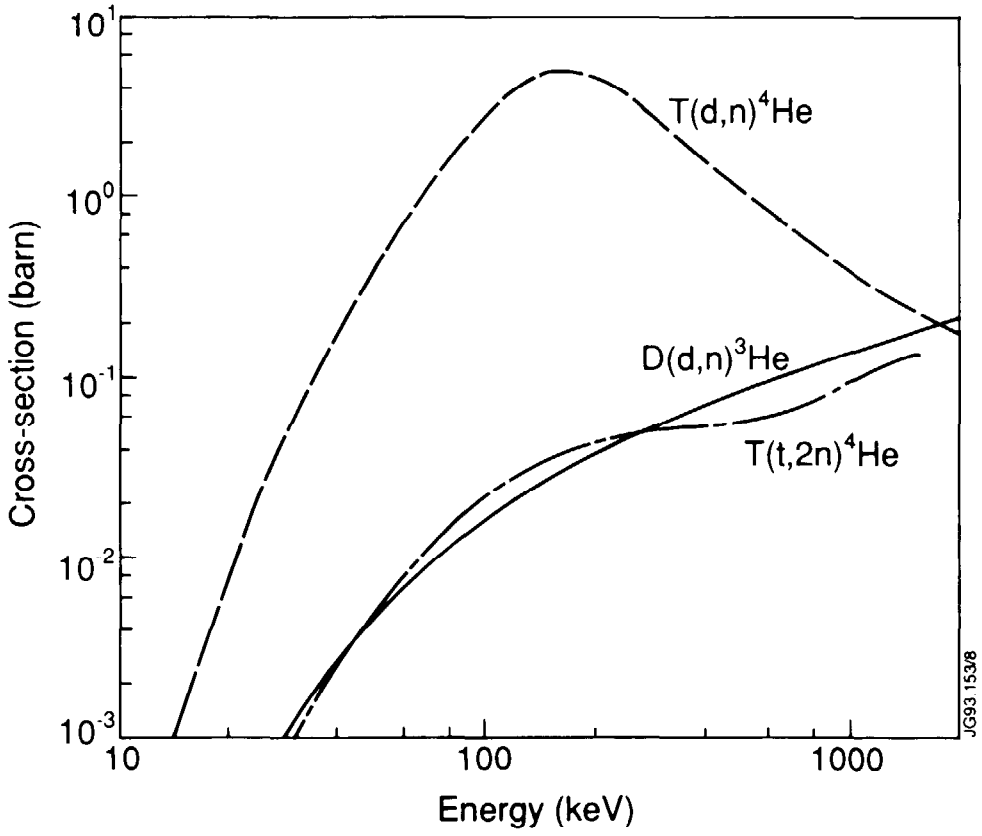

Fig.1: The variation of the total cross-section with energy for the three neutron-producing fusion reactions. The (thermal) target particles are denoted by upper-case letters and the bombarding particles, or projectiles, by lower-case letters. The projectile energy is given in keV for the laboratory frame of reference.

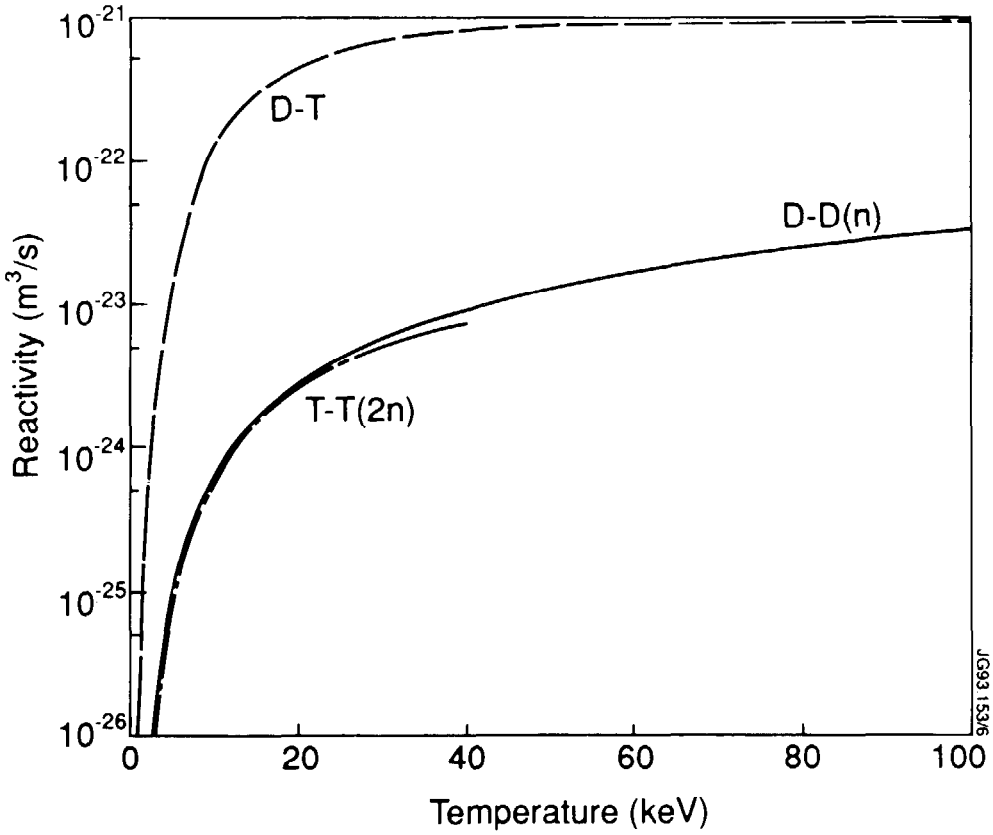

Fig.2: The variation of the reactivity with plasma temperature for the three neutron-producing reactions. A Maxwellian ion energy distribution is assumed.

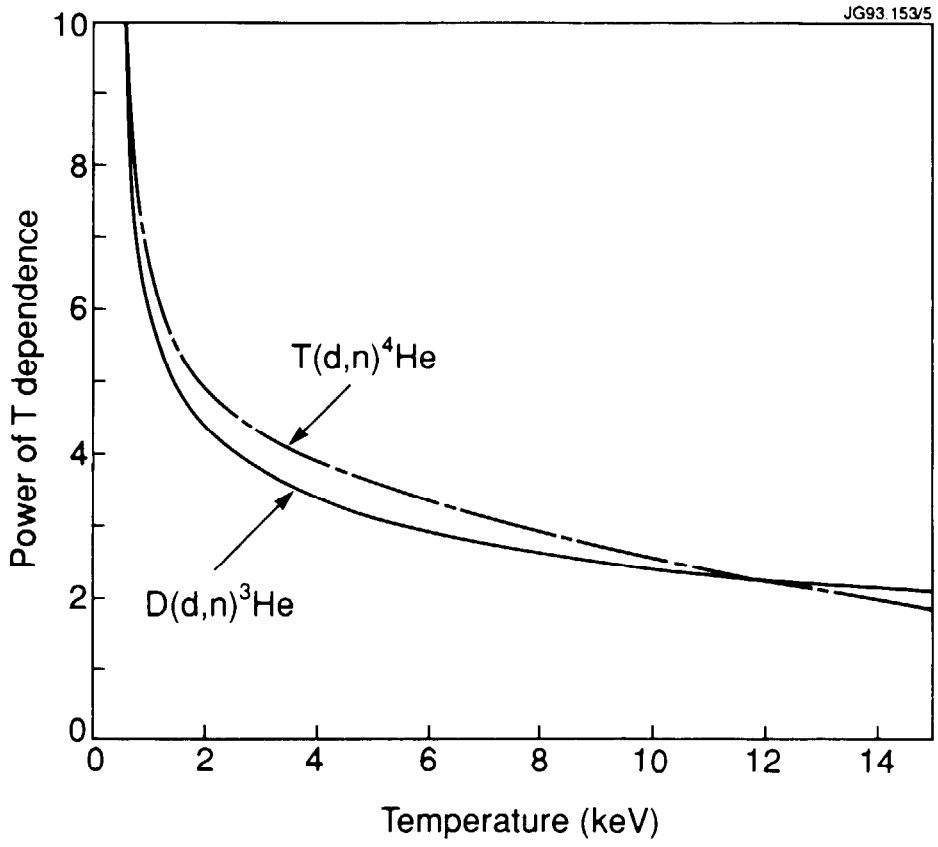

Fig.3: The variation of the exponent γ with plasma temperature for the D-D_n and D-T fusion reactivities when the plasma reactivity is described by the power dependence T_i^{γ}.

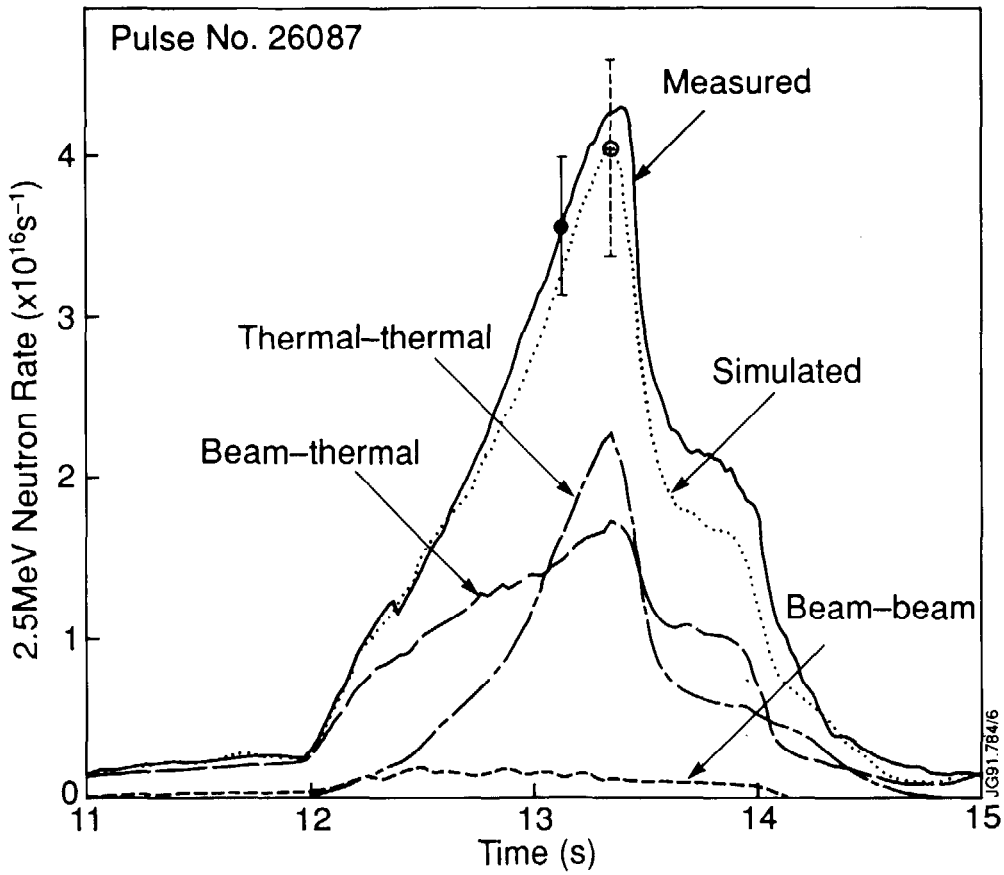

Fig.4: The time-dependence of the 2.5 MeV neutron emission for discharge number 26087; this is the highest d-d intensity yet achieved at JET . Discharge 26087 was one of a series preparatory to the first tritium discharges in JET (JET Team, 1992). The plasma was heated with 14 MW of deuterium NBI. The neutron emission as simulated with TRANSP is also shown, to indicate the relative rates due to thermal, beam-thermal and beam-beam fusion reactions.

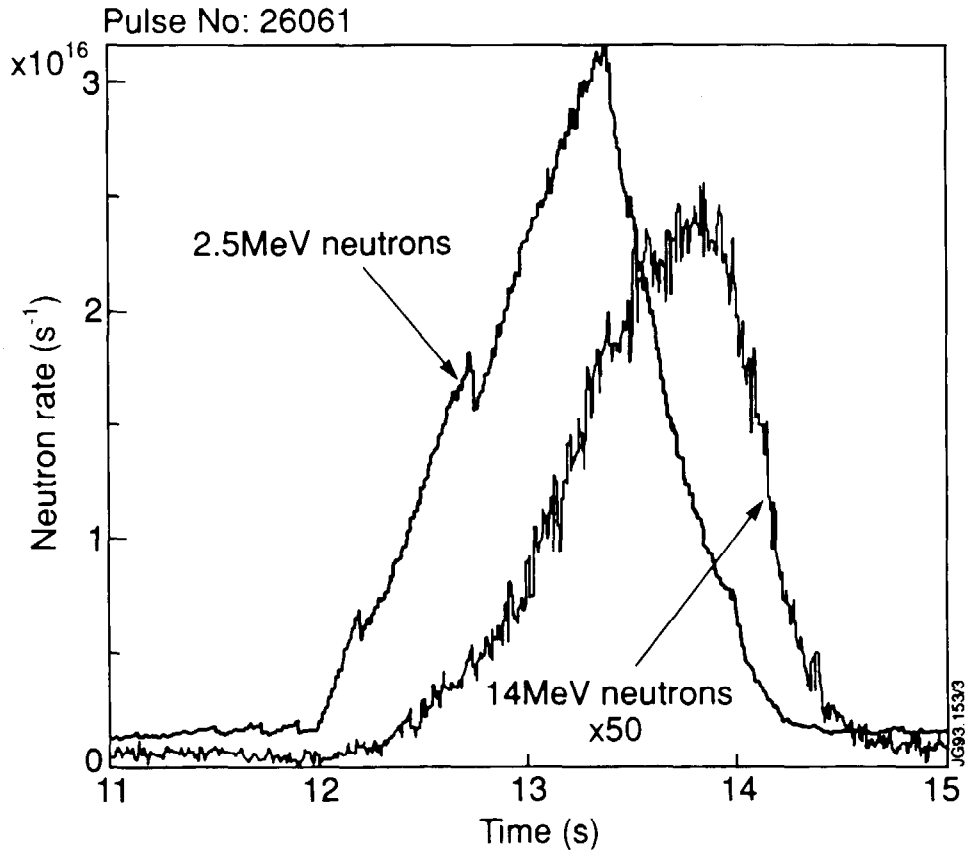

Fig.5: The 2.5 MeV neutron emission is compared with the 14 MeV neutron emission from triton burnup reactions, as measured with a silicon diode, for JET discharge 26061. The time delay between the source fusion reactions (the 2.5 MeV neutron signal) and the resulting burnup signal is clearly exhibited.

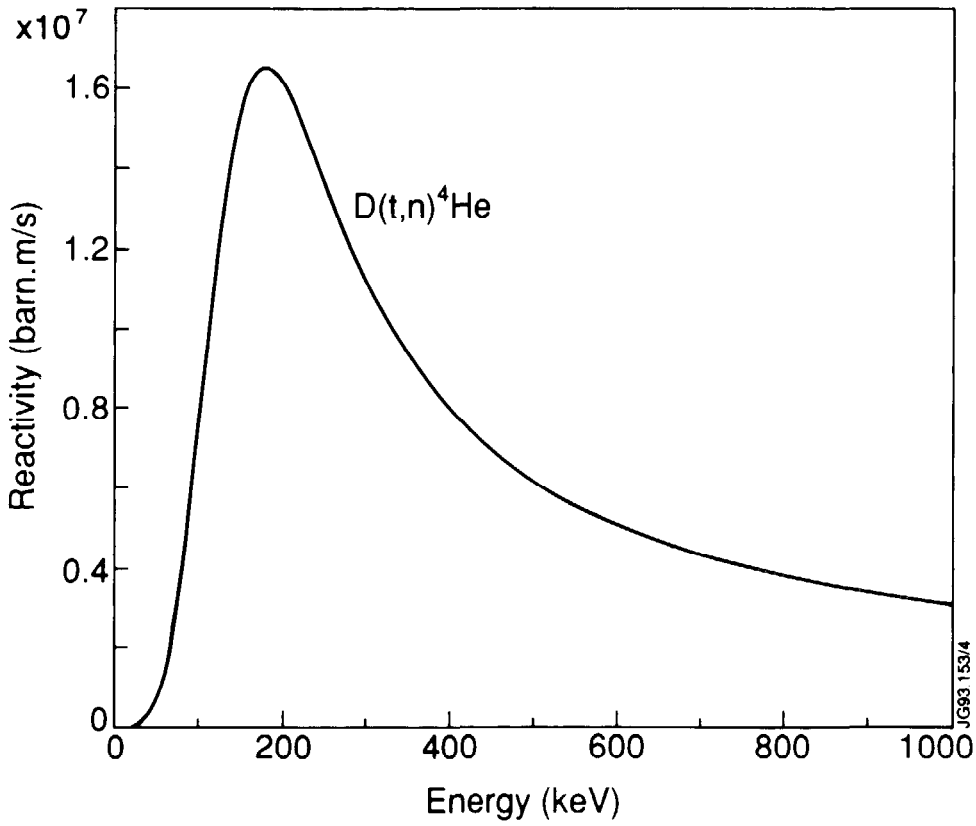

Fig.6: The variation of the t-D reactivity, $\langle\sigma v\rangle$, with triton (laboratory) energy for a cold target. The peak at about 180 keV is reached after the tritons have been slowing down (from 1.0 MeV) for, typically, about 300 ms in a hot plasma.

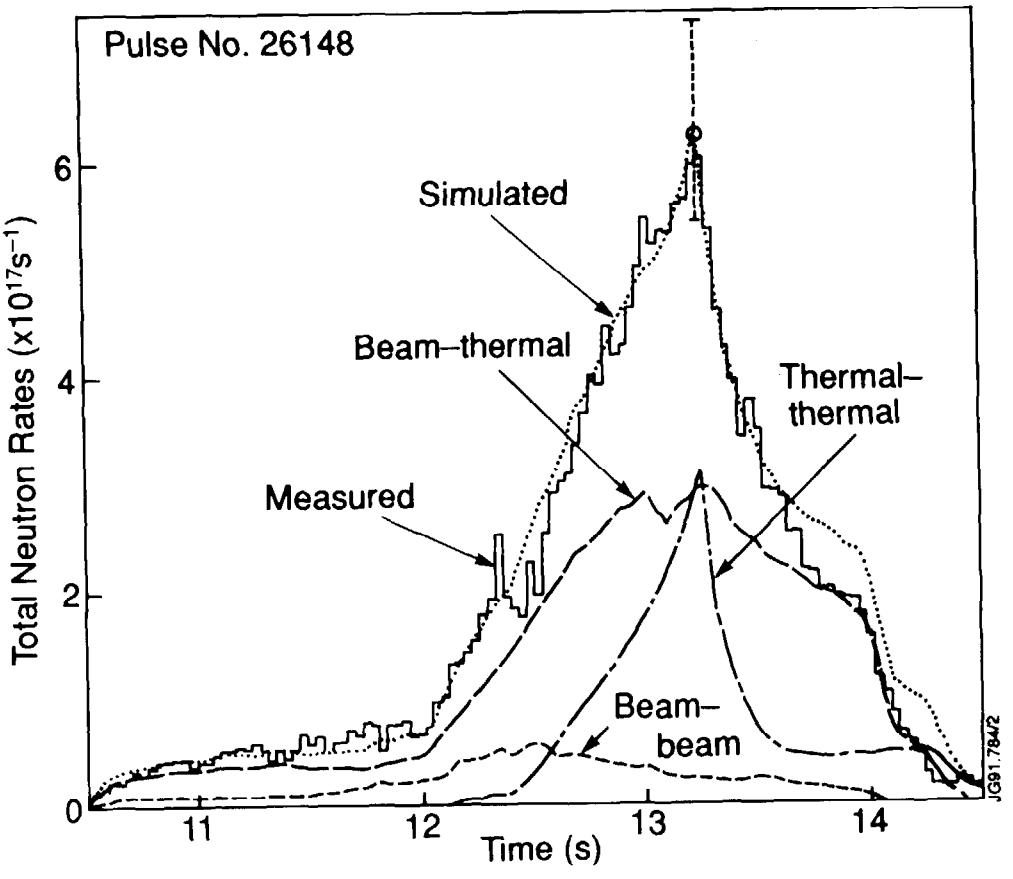

Fig.7: The time-dependence of the 14 MeV neutron emission from JET discharge 26148, the record intensity obtained from any tokamak to date (JET Team, 1992). For this discharge, 2 MW of deuterium NBI was replaced by 2 MW of tritium NBI. The neutron production rates due to thermal, beam-thermal and beam-beam fusion reactions derived from a TRANSP simulation are shown. As for discharge No. 26087 (fig. 4), the period of intense neutron emission was terminated by an influx of impurities from the surrounding structures.

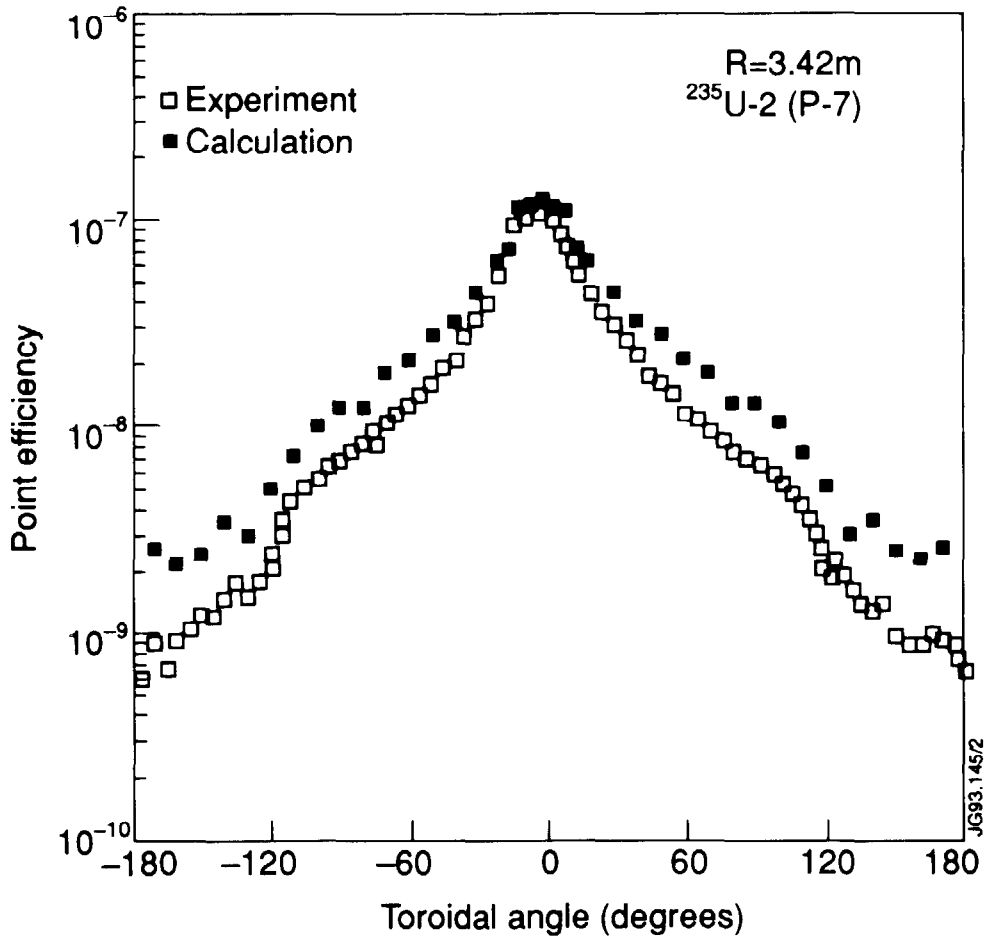

Fig.8: The dependence of neutron detector count-rate is shown as a function of toroidal position of a ^{252}Cf neutron point source in the JT-60U tokamak (from Nishitani et al., 1992). Integration of such data to simulate a plasma provides an accurate calibration of the detector response to deuterium plasma conditions. The predictions obtained with a neutron transport simulation are also shown.

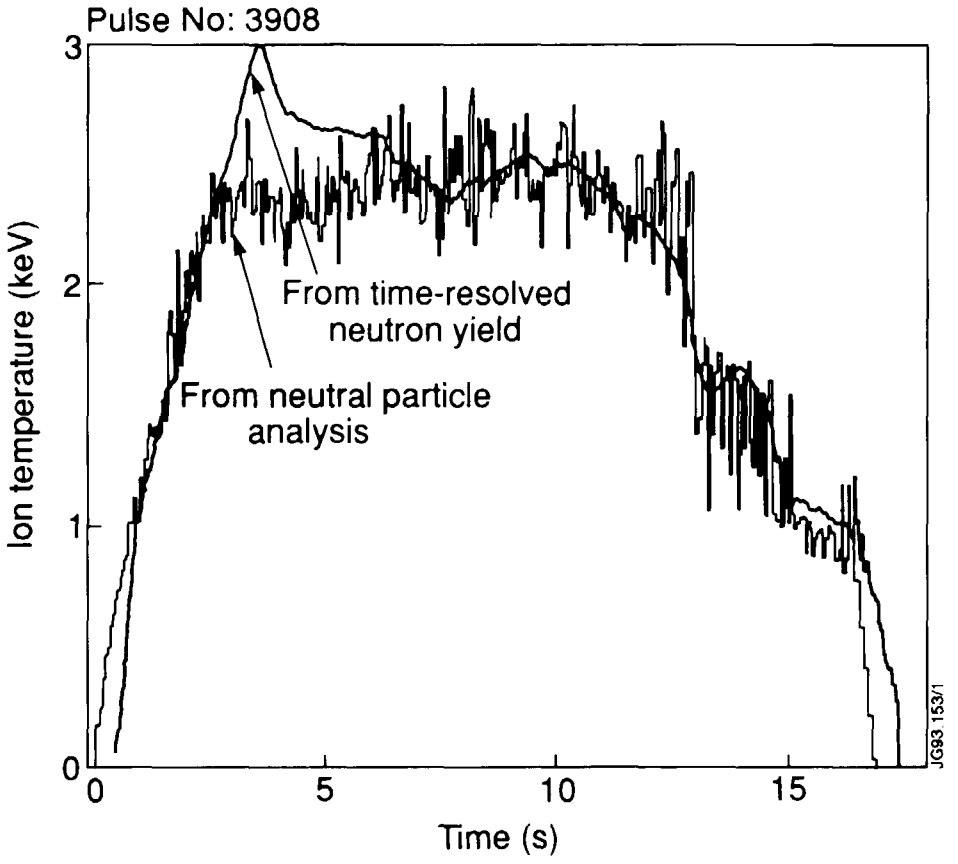

Fig.9: Comparison of ion temperatures from Neutral Particle Analysis and neutron yield measurements for JET discharge number 3908, using the value of 0.75 for the dilution ratio n_d/n_e derived from visible bremsstrahlung measurements.

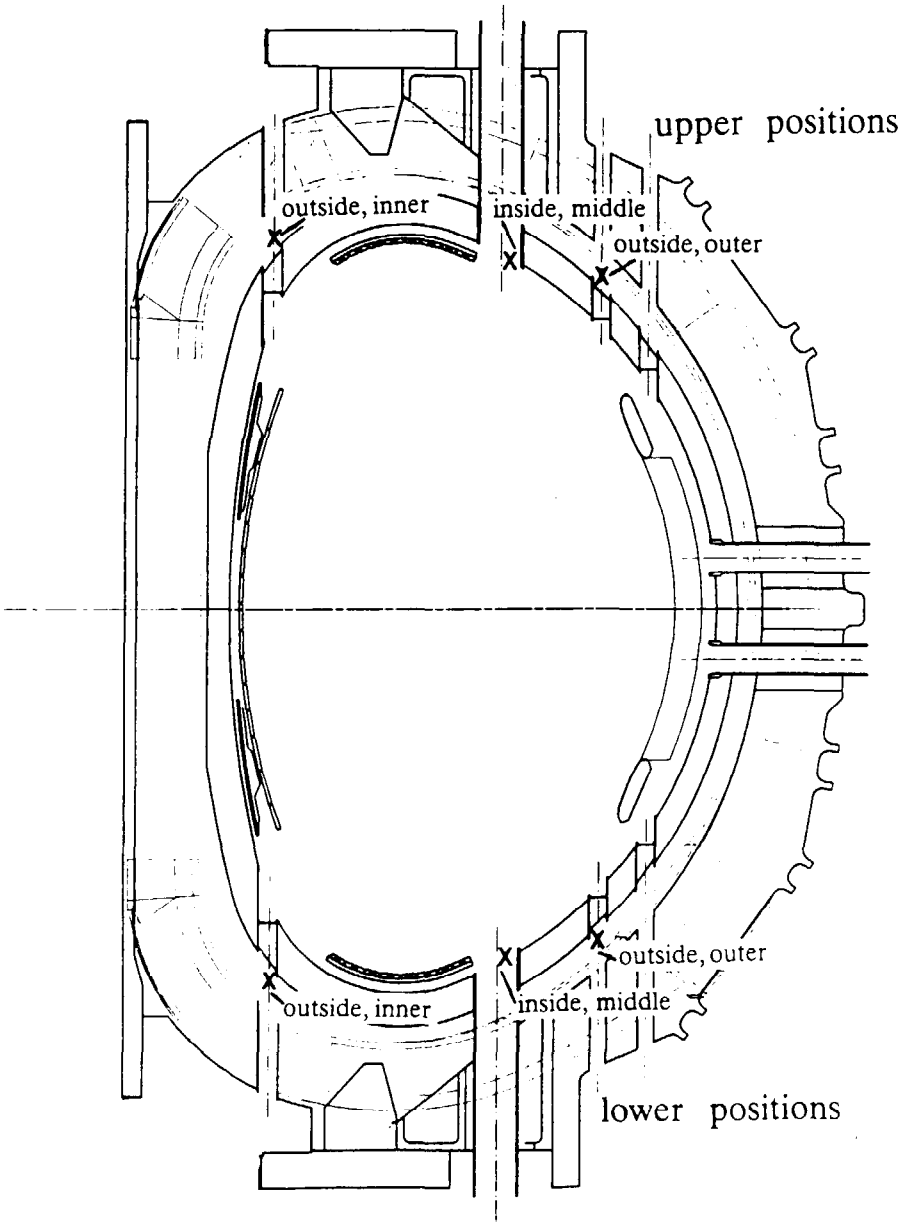

Fig.10: Showing a poloidal section through the JET tokamak to indicate the positions at which activation measurements may be obtained. There is mirror symmetry in the horizontal mid-plane.

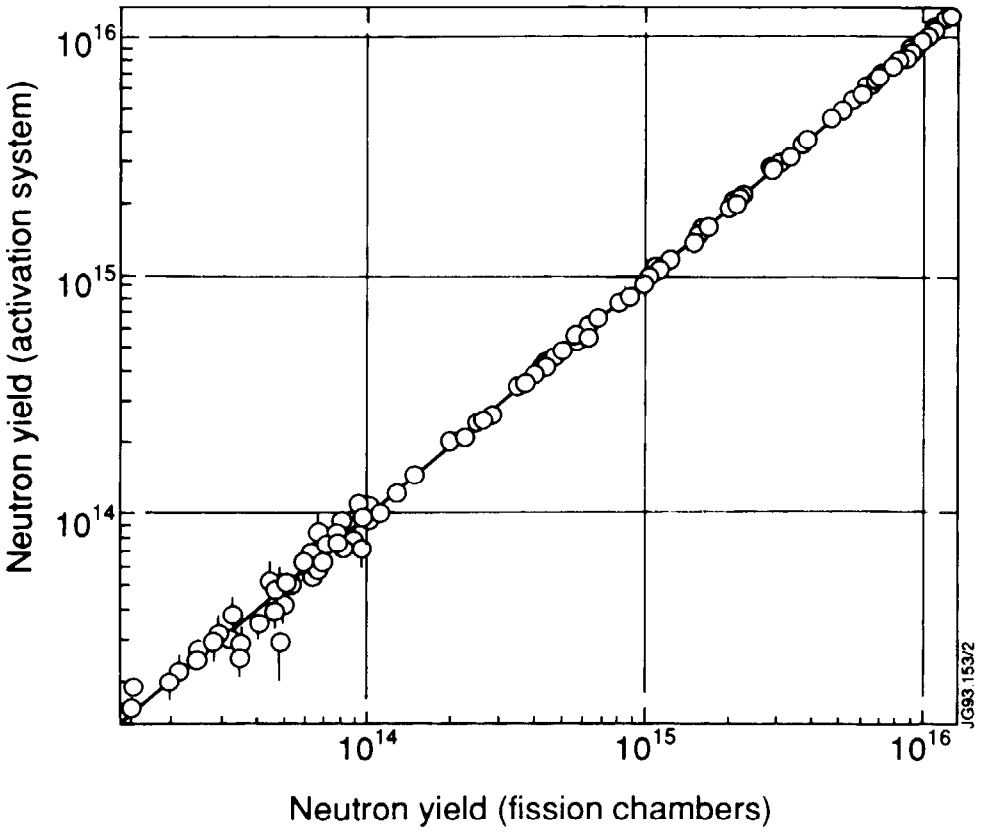

Fig.11: Demonstrating the high degree of linearity between the time-integrated neutron emission recorded by the JET fission chambers, calibrated at very low yields, with that obtained from activation measurements. The duration of the main period of neutron emission was typically about 1 second. For neutron yields in excess of 10^{14}, the statistical uncertainty in each measurement is much smaller than the plotting symbol.

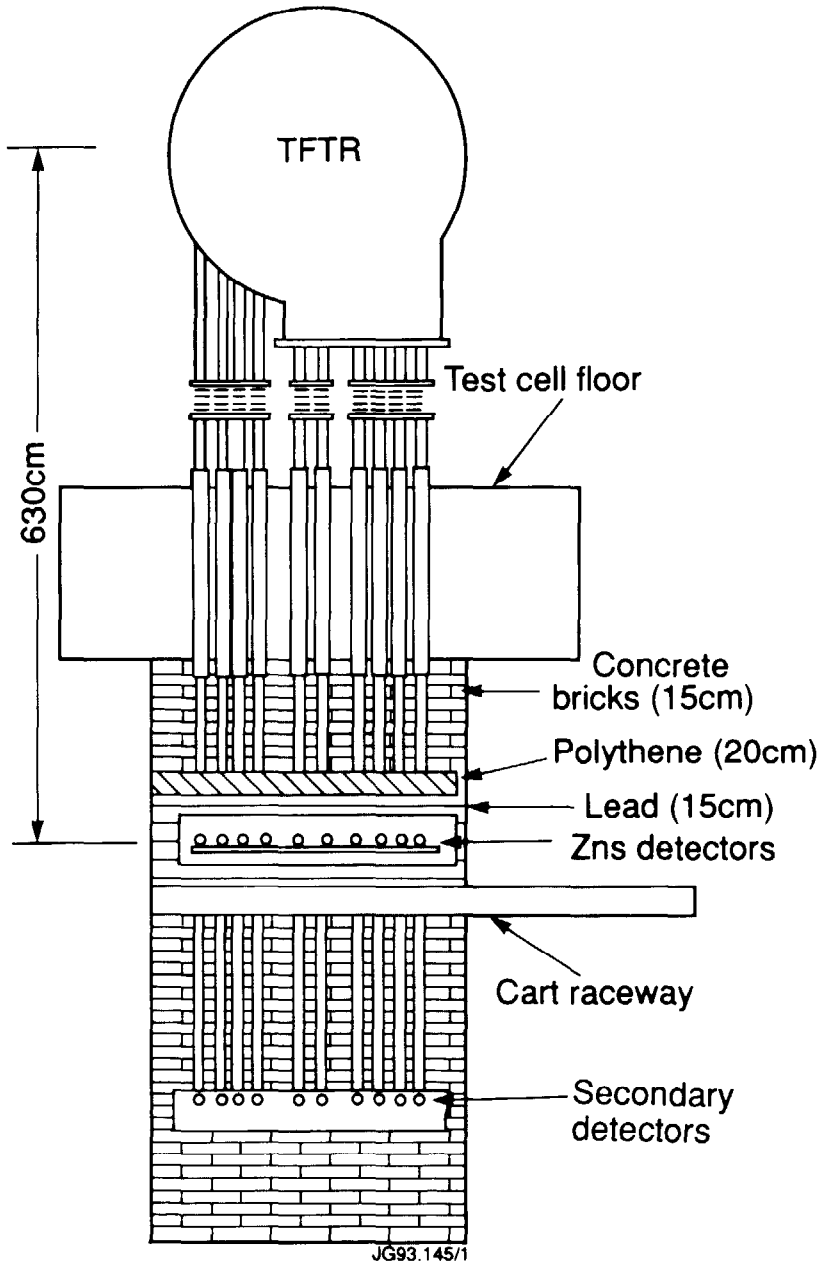

Fig.12: Elevation view of the TFTR multicollimator, showing the essential collimator components and the associated shielding (from Roquemore et al, 1990).

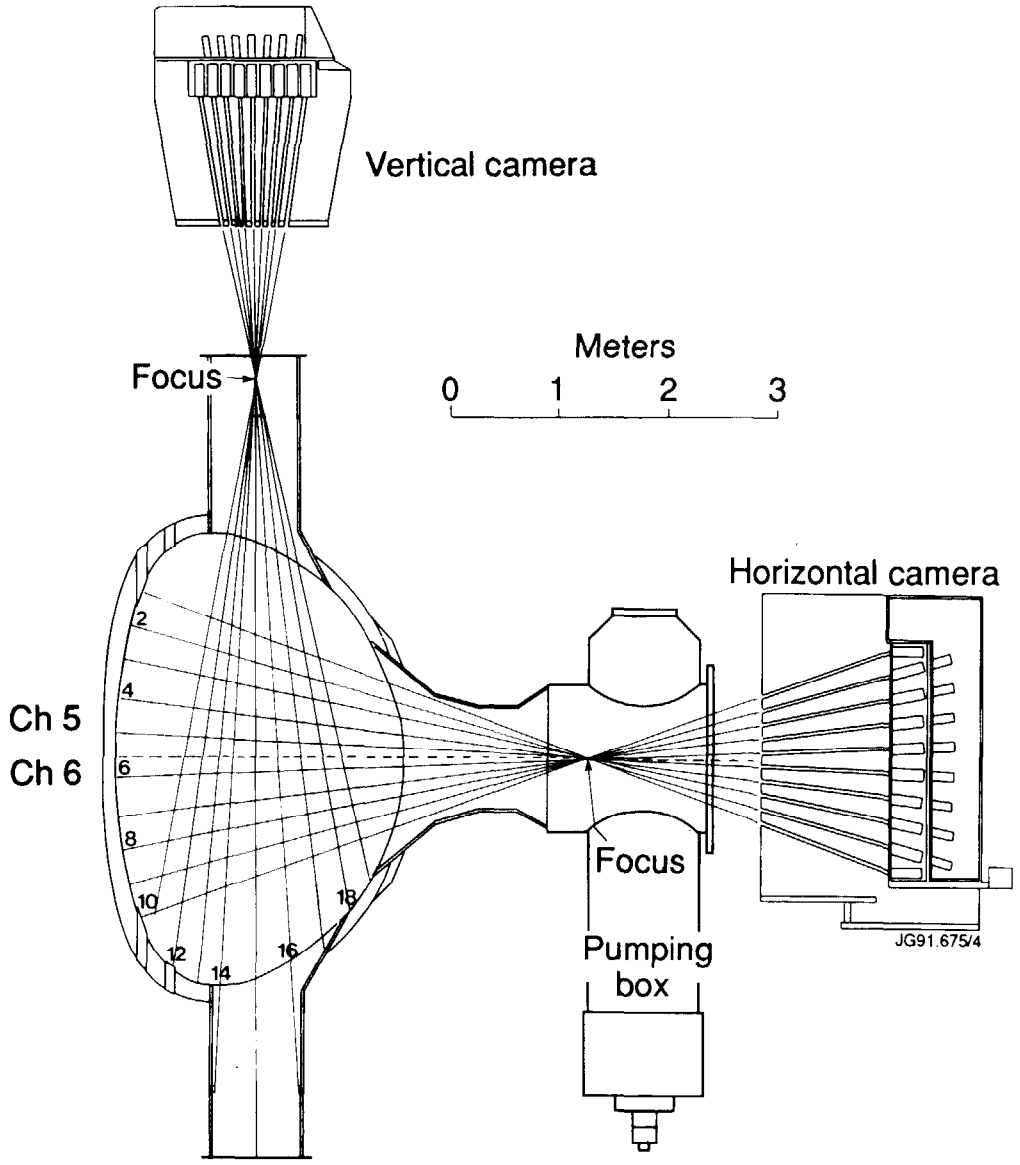

Fig.13: Illustrating the 19 lines-of-sight of the JET neutron profile monitor.

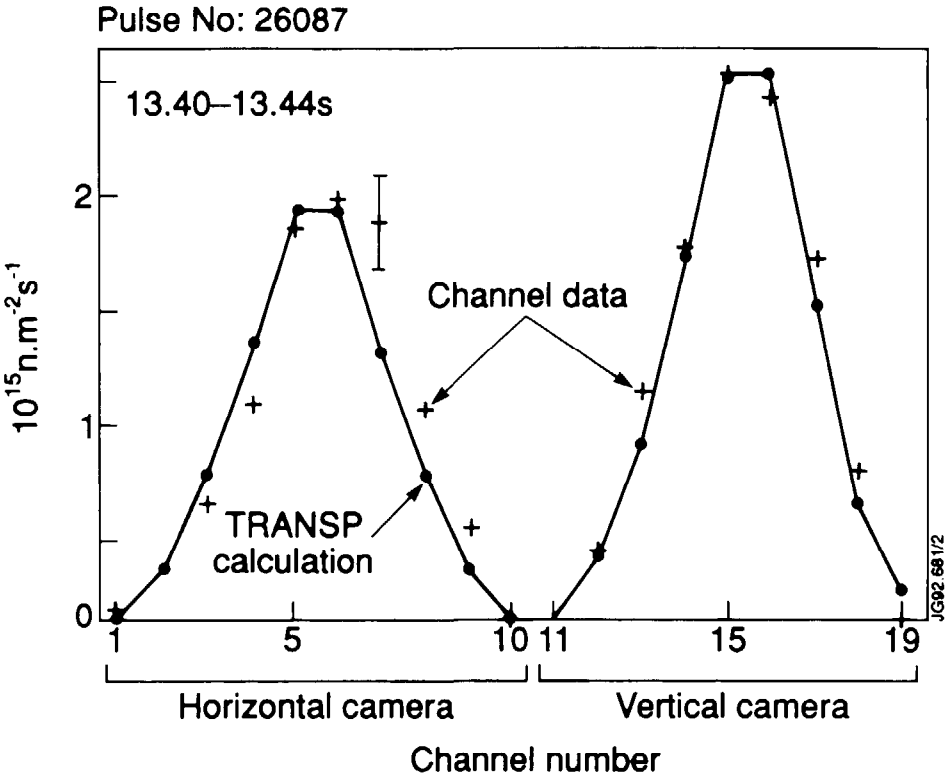

Fig.14: Neutron emission profiles for JET discharge No. 26087, taken at the moment of peak neutron emission. The line-integrated signals for each of the 19 channels are compared with predictions from the TRANSP code. (From Marcus et al., 1993).

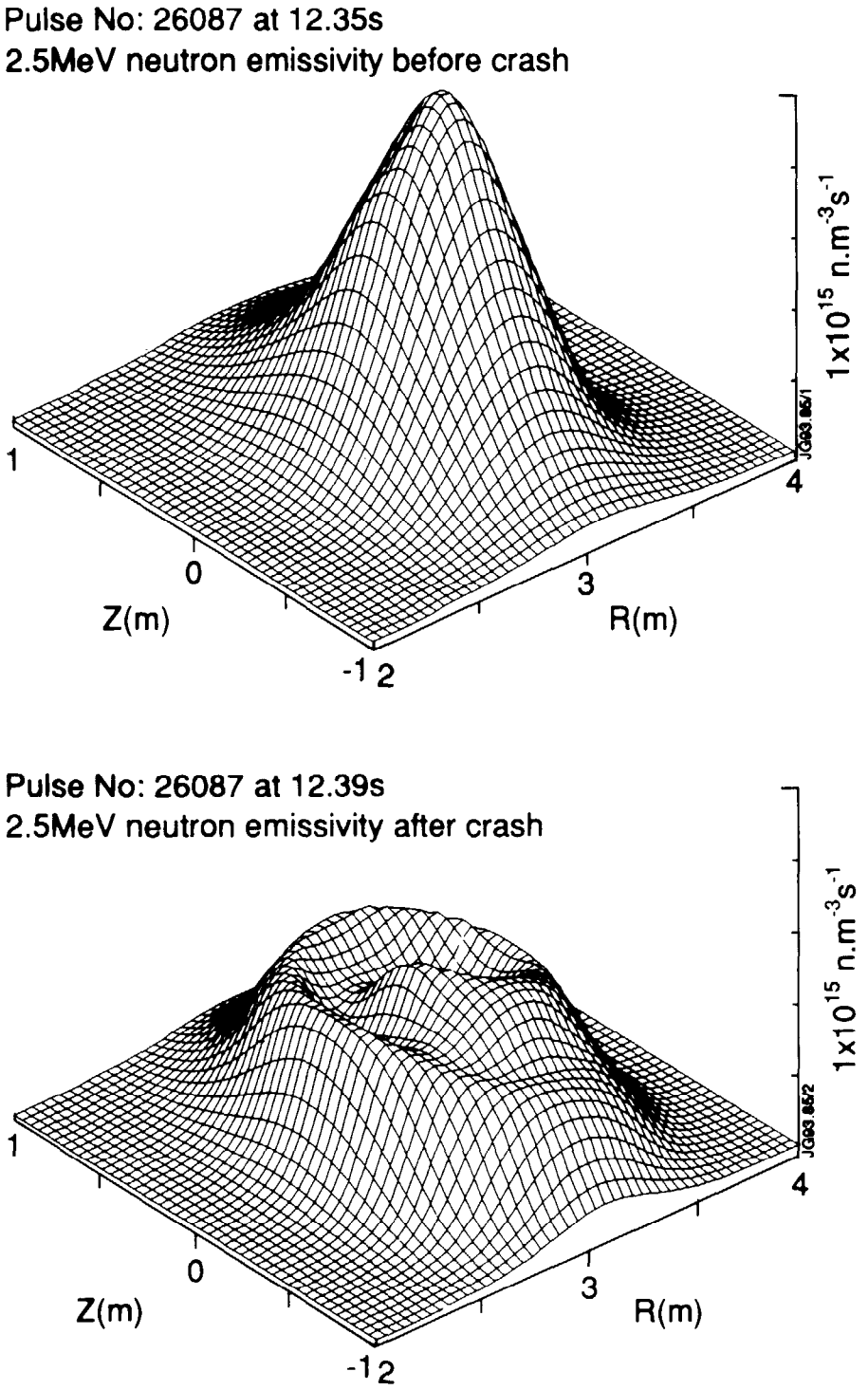

Fig.15: Tomographic analysis provides the 2-D emissivity plots for JET discharge No. 26087 for two periods: (upper) just before the sawtooth crash at 12.35 seconds, and (lower) just after the crash. (From Marcus et al., 1993).

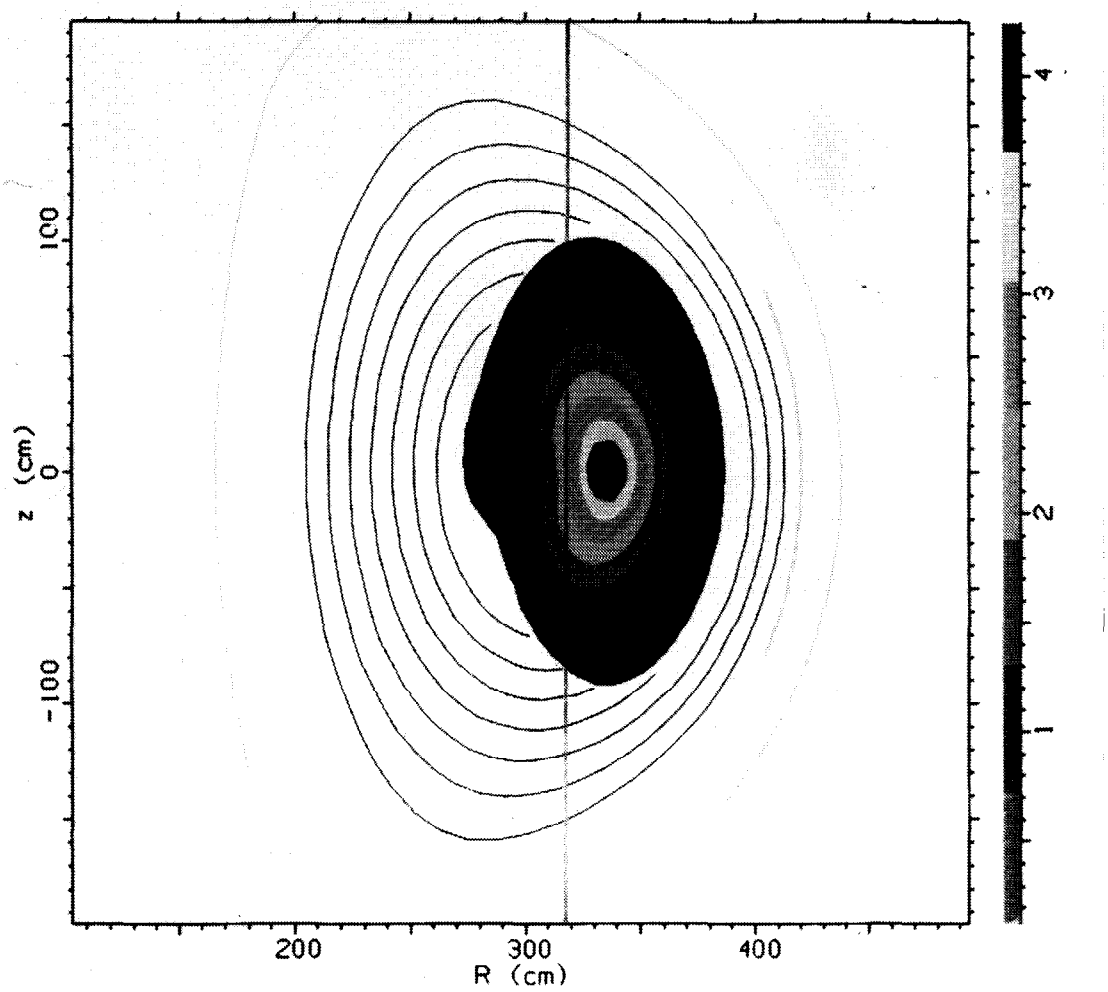

Fig.16: A contour plot of gamma-ray emissivity for an ICRF-heated discharge (JET discharge No. 23453) with resonance layer situated 16 cm from the plasma axis (Howarth et al., 1993). The gamma-rays are generated by nuclear interactions between fast ^{3}He ions and impurity ^{9}Be ions; there is an associated production of neutrons that has the same spatial origin. The positions of the magnetic flux surfaces are indicated. The fast ions possess a highly anisotropic velocity distribution and are trapped on the low field side of the resonance position.

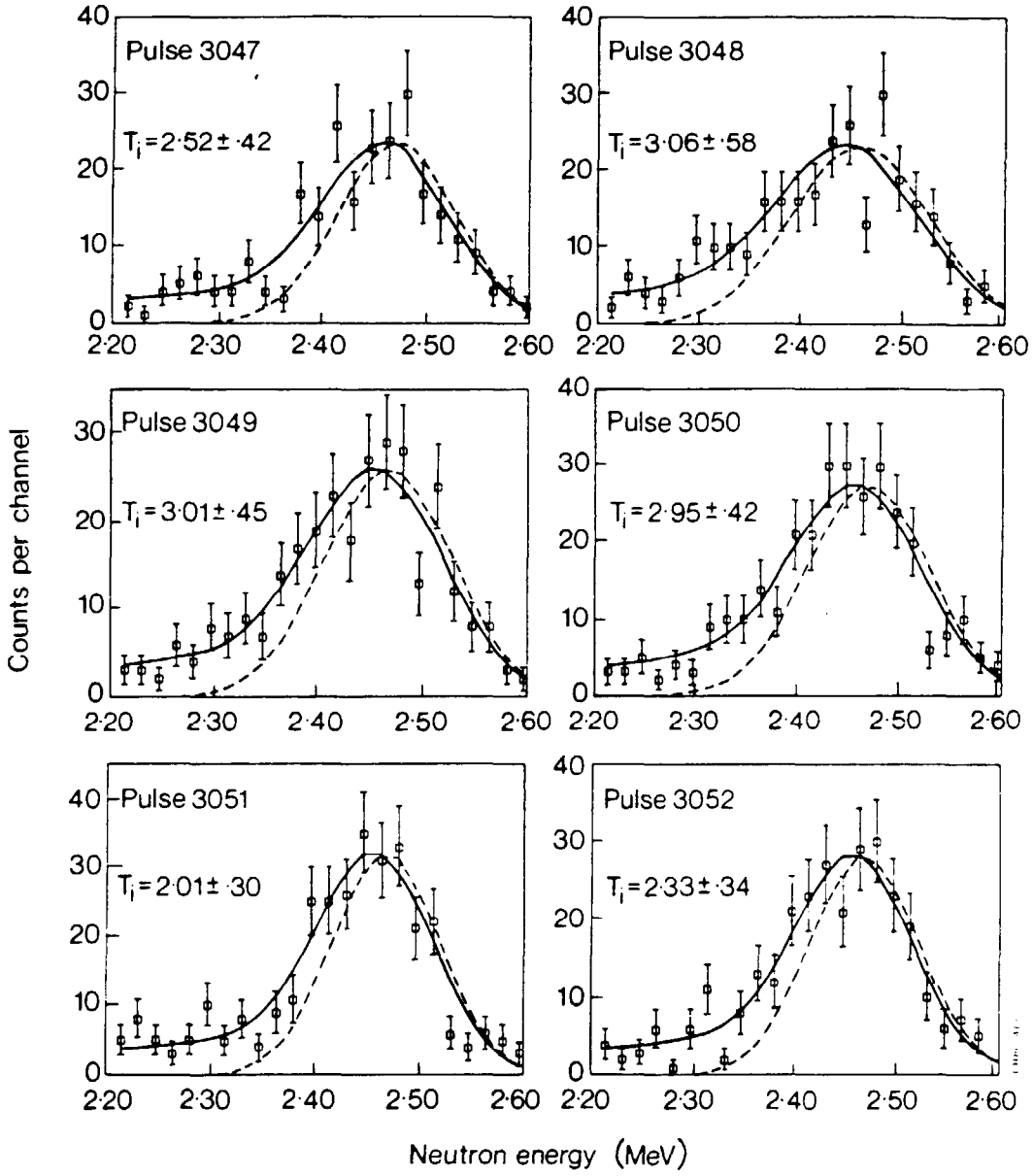

Fig.17: Neutron energy spectra taken at JET with a ^{3}He ionization chamber spectrometer (Jarvis et al., 1986). The period of integration for these spectra was 5 sec. or longer. The data are fitted with a variable-width gaussian folded into the detector response function to obtain the most probable ion temperature; the deduced temperatures at the centre of the plasma are shown, after correction for line-of-sight averaging.

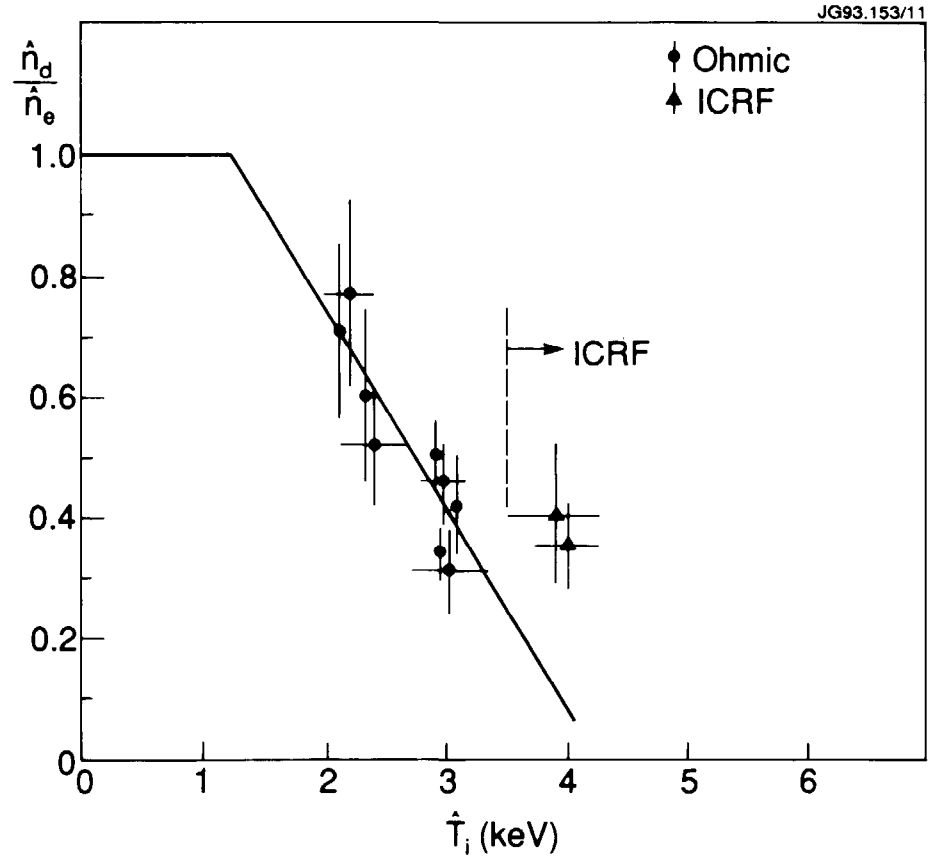

Fig.18: The variation of the dilution ratio n_d/n_e as a function of plasma temperature, for some ohmically heated deuterium discharges and two ICRF-heated discharges, with carbon limiters. The ion temperatures were derived from neutron spectra, as illustrated in fig 17, obtained using a ^{3}He ionization chamber spectrometer. (From Jarvis et al., 1987).

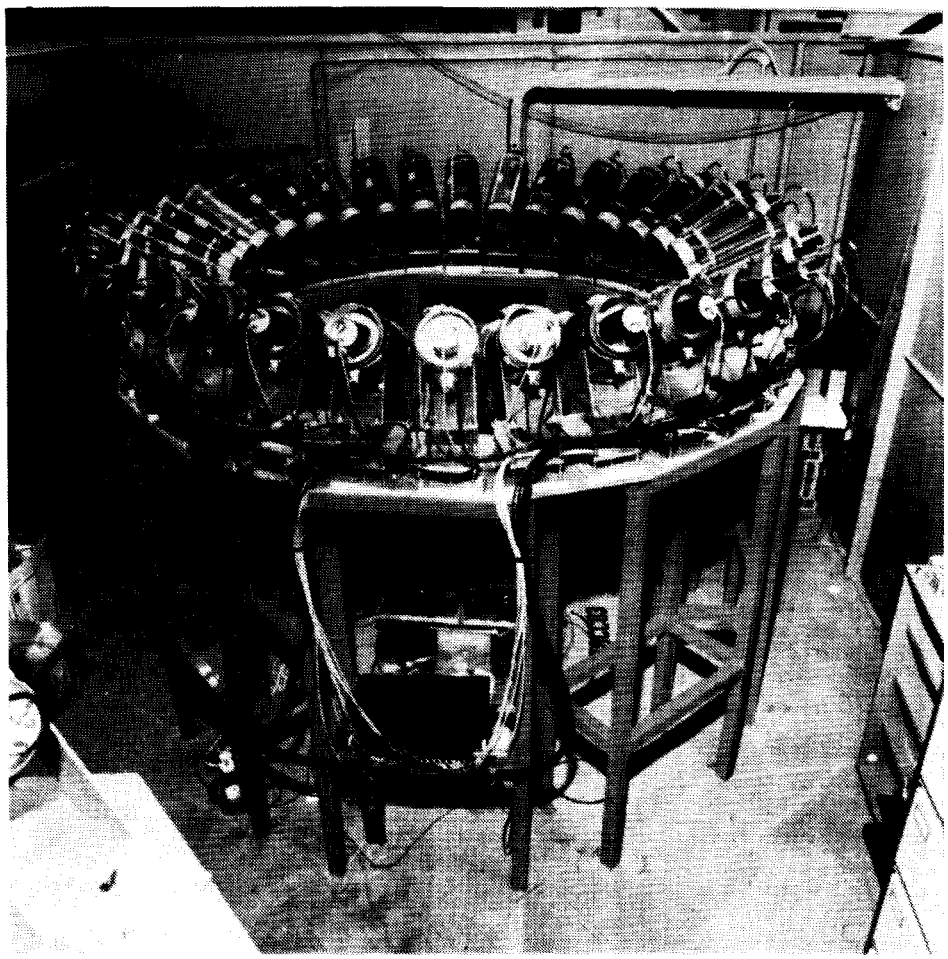

Fig.19: Photograph of the JET 2.5 MeV neutron time-of-flight spectrometer. The neutron beam is defined by a vertical collimator set into the floor, and pass through the scintillator placed close to the floor, on the axis of the 32-detector array.

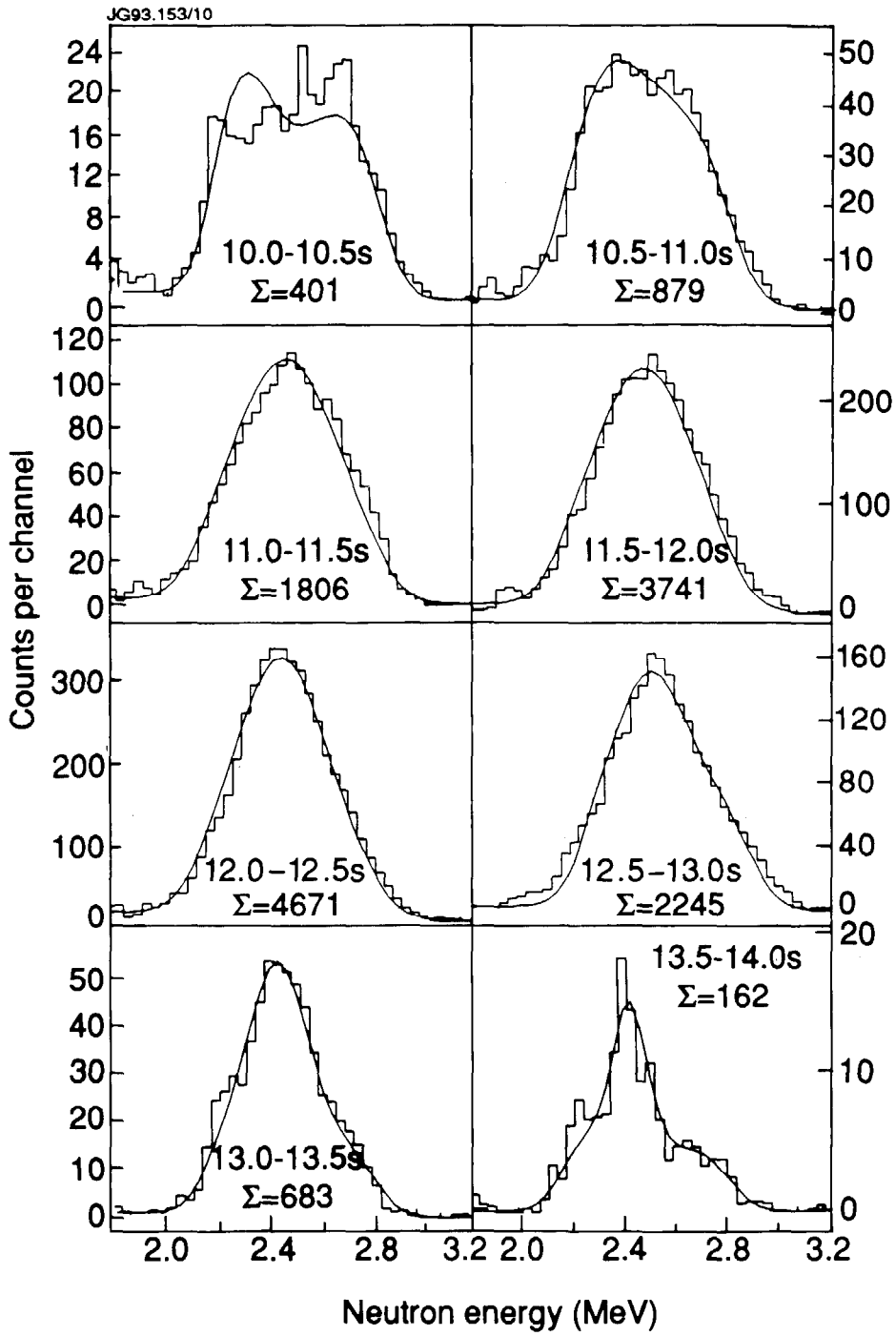

Fig.20: Neutron energy spectra obtained with the JET 2.5 MeV neutron time-of-flight spectrometer for NBI-heated discharge No. 25432, to illustrate the high count-rate capability. Analysis (the fitted curves) permits the relative proportions of thermal to beam-plasma reaction rates to be determined, based on ion temperatures from X-ray spectroscopy. The first spectrum corresponds to beam-plasma reactions in a cold plasma; subsequent spectra show the ion temperature rising to apeak at about 18 keV, when thermal, beam-plasma and beam-beam reactions are of comparable magnitude; the final spectra show the rapid collapse of the temperature and neutron yield due to an uncontrolled influx of impurities. (From Elevant et al., 1992).

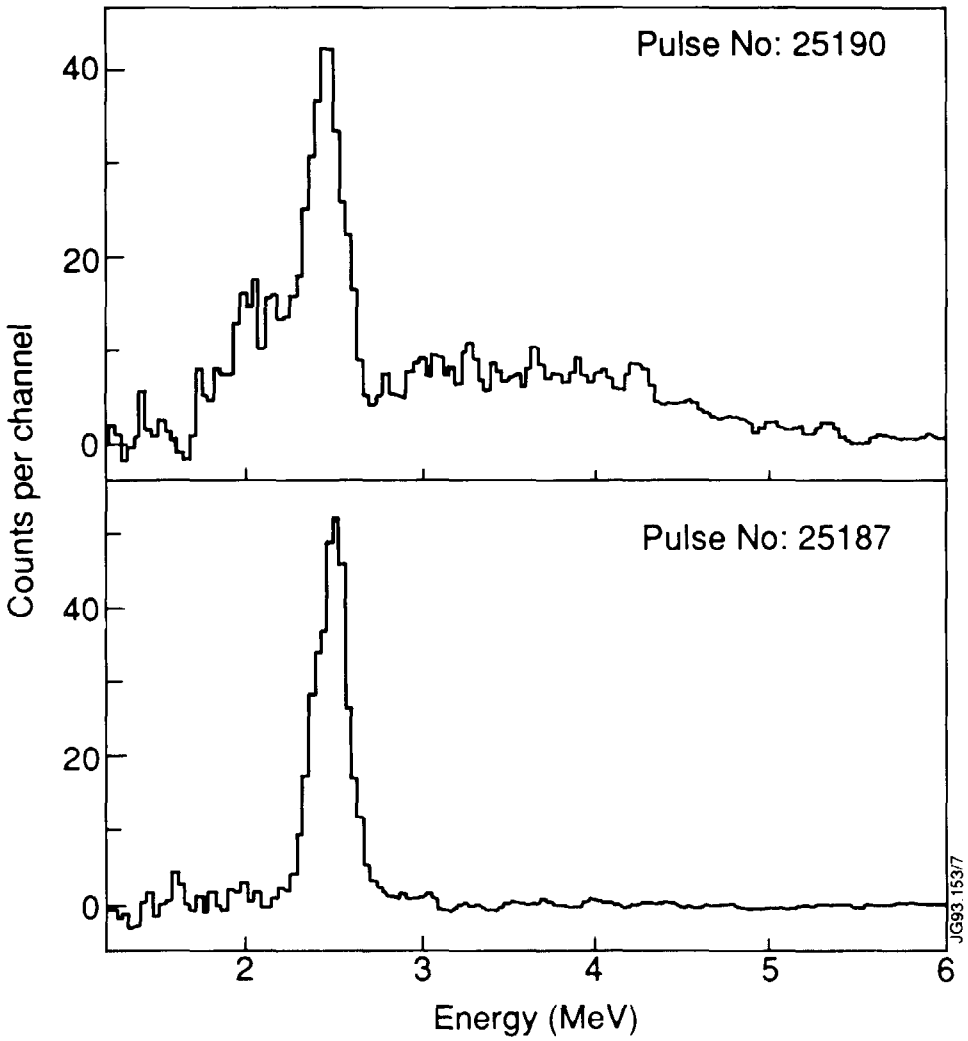

Fig.21: Neutron energy spectra obtained with the JET 2.5 MeV neutron time-of-flight spectrometer for two similar discharges with combined NBI and ICRF heating; in discharge No. 25190, the plasma conditions are such that the ICRF generates a fast proton population that produces high energy neutrons from interactions with ^{9}Be impurity ions. A random coincidence count-rate subtraction has been made.

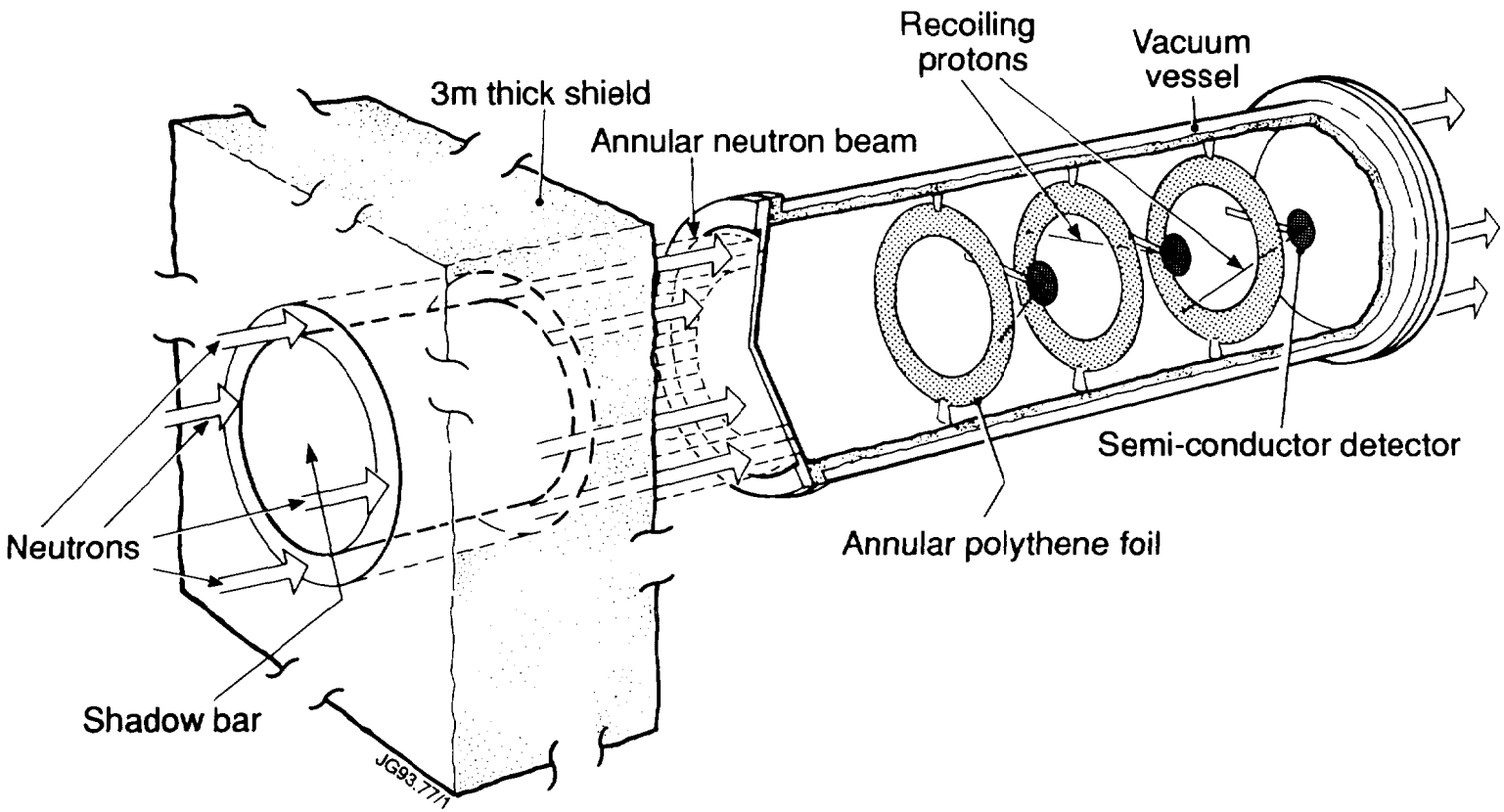

Fig.22: Illustrating the principle of the JET tandem radiator spectrometer. The annular flux of neutrons passes through the three polythene foils; protons recoiling at small angles may be detected by the silicon diodes placed on the axis of symmetry of the instrument. The diodes are protected from the incident neutrons by means of a shadow bar set in the 2-m thick shield wall.

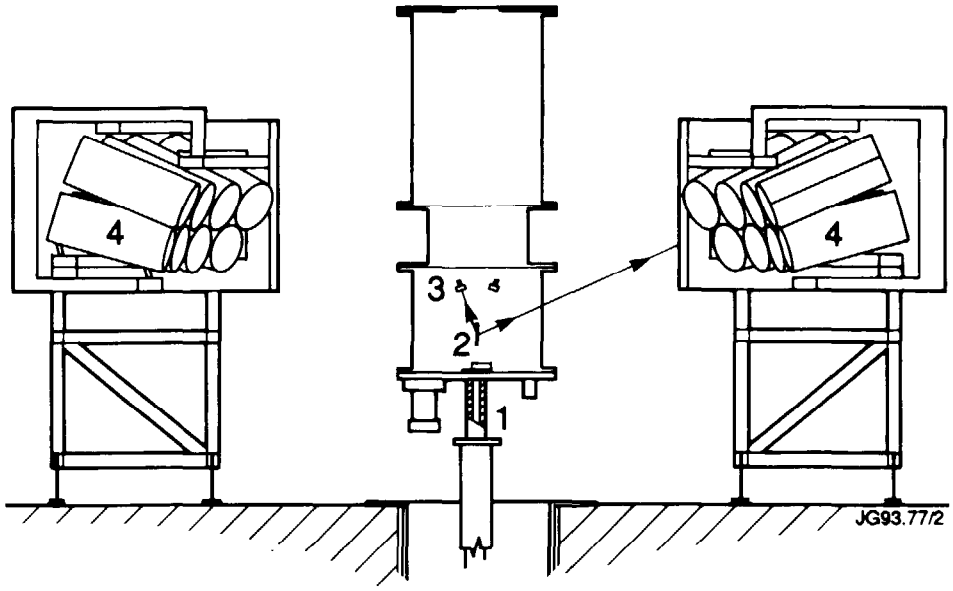

Fig.23: Illustrating the principle of the JET associated particle neutron time-of-flight spectrometer. Source neutrons enter vertically through the collimator (1); scattering occurs in the polyethylene foil (2). The recoil protons are detected in the 6 proton detectors (3) located inside the vacuum chamber and the associated scattered neutrons are recorded in coincidence in the two banks of 16 neutron detectors (4). (From Grosshoeg et al., 1987).